

1 Author response to reviewers.

2 **Biomass burning at Cape Grim: exploring**
3 **photochemistry using multi-scale modelling**

4 Sarah J. Lawson, Martin Cope, Sunhee Lee, Ian E. Galbally, Zoran Ristovski and Melita D.

5 Keyword

6 ACP-2016-932

7 Authors response are denoted by >>

This paper performs a thorough evaluation CTM utilising two independent meteorological models to investigate the impact of two biomass burning events measured at Cape Grimm. The paper has been considerably improved following the earlier draft. It reads better, is clearer and more consistent in terminology, performs a more thorough meteorological evaluation and contains better analysis of the chemical history and production of O₃ under the different scenarios. With a few minor changes as detailed below, the paper will be suitable for publication.

General

comment:

It is good to see that there has been a more thorough, statistical meteorological and chemical evaluation. However, quite a lot has been relegated to the supplement. In general, I think any figure which is discussed in detail in the main paper in order to further the story should be included in the main paper, and only those figures which just add further evidence for the story and are not essential to it be put in the supplement. I would suggest the following are discussed in detail in the text, and so should be in the main paper:

S18. Wind direction plots for BB2, when evaluating sensitivity of plume detection to meteorology, in section 3.1.1

>>as requested has been moved to main paper (Fig 5).

S11. Quantile-quantile plots for BC and CO, as discussed in section 3.1.1

>>as requested has been moved to main paper (Fig 8) Some minor formatting changes have been made (symbol size etc) to improve clarity

S14. Quantile-Quantile plots of O₃, as discussed in section 3.1.1

>>as requested has been moved to main paper (Fig 9) Some minor formatting changes have been made (symbol size etc) to improve clarity

Specific

comments:

Abstract – Note that the model produced spurious O₃ titration events with higher MCEs, and performed best when MCE = 0.89 (close to observed). Highlight the importance of simulating transport and using back-trajectories (as in last paragraph on conclusion) in simulating O₃ production, as you show the ozone production was due to Melbourne rather than the BB fire.

>> to abstract have added “This work also shows the importance of using models to elucidate the contribution from different sources to atmospheric composition, where this is difficult using observations alone.”

Ln 98. Delete second ‘.’
>>done

Ln 100. Take Giglio et al. out of brackets.
>>done

Ln 154. Please give a few references for other studies which vary emissions ‘linearly’. Please clarify – you mean by scaling emissions of all species by a constant factor?
>>yes. Changed text to “which typically scale emissions of all species by a constant factor” and added references Lei et al., 2013 and Pacifico et al., 2015

Ln 221-236. Please refer to Figure 1 somewhere in this paragraph when discussing domains.
>>the following sentence has been added “ Figure 1 shows the five nested computational domains used in TAPM-CTM and CCAM-CTM.”

Ln. 255. Delete ‘T’
>>done

Ln 275. Reorder sentence: “Savanna category EFs from Andreae and Merlot (2001) were used as base case EFs in this work.”
>>this line has been removed based on reviewer comment further down (Ln 275-293)

Ln 278. ‘Used published’
>>done

Ln 275-293. You repeat several things unnecessarily in these two paragraphs, e.g. you state the lower (0.89), best estimate (0.92) and upper (0.95) MCEs several times. I think these two paragraphs could be merged into one to make more concise.
>>the first paragraph describes how the 3 MCE’s were calculated, while the second paragraph describes how EF were derived for each of the MCEs. These paragraphs were rewritten in response to comments from the other two reviewers to clarify how the EF used in the model were derived. In response to this reviewer we have removed the values of 0.89, 0.92 and 0.95 which are repeated several times, and have removed the first line of paragraph 1 to simplify the text.

Ln 348. “BB1 and”
>>done

Ln 352. Delete space between “(Figure 5) .”

>>done

Figure 4 & 5. It would be good if you could present the panels for the two simulations side-by-side, as they are really quite different. In the interest of saving space, I would suggest presenting as one Figure, with a column from each CTM. I think you can remove the panels for 18 Feb 04:00, and maybe 15 Feb 16:00, without too much lost information. Please also add panels of wind direction timeseries compared to observations, similar to in Figure S18. In reference to the earlier comment, Figure S18 could then be the new Figure 5.

>>as suggested Figures 4 and 5 have been merged so panels are side by side (now Fig 4). As requested the wind direction time series for this Figure has been added above the concentration isopleths. As suggested Figure S18 is now Fig 5 (see above). The two TAPM-CTM and CCAM-CTM wind direction time series on Fig 5 have been merged to a single time series, to be consistent with the format for Fig 4.

8

9

10

11 **Biomass burning at Cape Grim: exploring photochemistry**
12 **using multi-scale modelling**

13 **Sarah J. Lawson¹, Martin Cope¹, Sunhee. Lee[†], Ian E. Galbally¹, Zoran Ristovski²**
14 **and Melita D. Keyword¹**

15 [1] Commonwealth Scientific and Industrial Research Organisation, Climate Science Centre,
16 Aspendale, Australia

17 [2] International Laboratory for Air Quality & Health, Queensland University of Technology,
18 Brisbane, Australia

19 [†]decreased

20 Correspondence to: S. J. Lawson (sarah.lawson@csiro.au)

21

22 **Abstract**

23 We have tested the ability of a high resolution chemical transport model (CTM) to reproduce
24 biomass burning (BB) plume strikes and ozone (O₃) enhancements observed at Cape Grim in
25 Tasmania Australia from the Robbins Island fire. The CTM has also been used to explore the
26 contribution of near-field BB emissions and background sources to O₃ observations under
27 conditions of complex meteorology. Using atmospheric observations, we have tested model
28 sensitivity to meteorology, BB emission factors (EF) corresponding to low, medium and high
29 modified combustion efficiency (MCE) and spatial variability. The use of two different
30 meteorological models (TAPM-CTM and CCAM-CTM) varied the first (BB1) plume strike
31 time by up to 15 hours, and duration of impact between 12 and 36 hours, and varied the second
32 (BB2) plume duration between 50 and 57 hours. Meteorology also had a large impact on
33 simulated O₃, with one model (TAPM-CTM) simulating 4 periods of O₃ enhancement, while
34 the other model (CCAM) simulating only one period. Varying the BB EFs, which in turn
35 varied the non-methane organic compound (NMOC) / oxides of nitrogen (NO_x) ratio, had a
36 strongly non-linear impact on simulated O₃ concentration, with either destruction or production
37 of O₃ predicted in different simulations. As shown in previous work (Lawson et al., 2015),
38 minor rainfall events have the potential to significantly alter EF due to changes in combustion
39 processes. Models which assume fixed EF for O₃ precursor species in an environment with
40 temporally or spatially variable EF may be unable to simulate the behaviour of important
41 species such as O₃.

42 TAPM-CTM is used to further explore the contribution of the Robbins Island fire to the
43 observed O₃ enhancements during BB1 and BB2. Overall, TAPM-CTM suggests the dominant
44 source of O₃ observed at Cape Grim was aged urban air (age = 2 days), with a contribution of
45 O₃ formed from local BB emissions.

46 This work shows the importance of assessing model sensitivity to meteorology and EF, and the
47 large impact these variables can have in particular on simulated destruction or production of
48 O₃ in regional atmospheric chemistry simulations. This work also shows the importance of
49 using models to elucidate the contribution from different sources to atmospheric composition,
50 where this is difficult using observations alone.

54 1 Introduction

55 Biomass burning (BB) makes a major global contribution to atmospheric trace gases and
56 particles with ramifications for human health, air quality and climate. Directly emitted species
57 include carbon monoxide (CO), carbon dioxide (CO₂), oxides of nitrogen (NO_x), primary
58 organic aerosol (POA), non-methane organic compounds (NMOC) and black carbon (BC),
59 while chemical transformations occurring in the plume over time lead to formation of
60 secondary species such as O₃, oxygenated NMOC and secondary aerosol. Depending on a
61 number of factors, including magnitude and duration of fire, plume rise and meteorology, the
62 impact of BB plumes on human health, air quality and climate may be local, regional or global.

63 BB plumes from wildfires, prescribed burning, agricultural and trash burning can have a major
64 impact on air quality in both urban and rural centres (Keywood et al., 2015; Luhar et al., 2008;
65 Reisen et al., 2011; Emmons et al., 2010; Yokelson et al., 2011) and regional scale climate
66 impacts (Andreae et al., 2002; Keywood et al., 2011b; Artaxo et al., 2013; Anderson et al.,
67 2016). In Australia, BB from wild and prescribed fires impacts air quality in both rural and
68 urban areas (Keywood et al., 2015; Reisen et al., 2011; Luhar et al., 2008; Keywood et al.,
69 2011a) as well as indoor air quality (Reisen et al., 2011). More generally, as human population
70 density increases, and as wildfires become more frequent (Flannigan et al., 2009; Keywood et
71 al., 2011b), assessing the impact of BB on air quality and human health becomes more urgent
72 (Keywood et al., 2011b; Reisen et al., 2015). In particular, particles emitted from BB frequently
73 lead to exceedances of air quality standards, and exposure to BB particles has been linked to

74 poor health outcomes including respiratory effects, cardiovascular disease and mortality
75 (Reisen et al., 2015; Reid et al., 2016; Dennekamp et al., 2015). There is also increasing
76 evidence that mixing of BB emissions with urban emissions results in enhanced
77 photochemistry and production of secondary pollutants such as secondary aerosol and O₃ (Jaffe
78 and Wigder, 2012; Akagi et al., 2013; Hecobian et al., 2012), which may result in more
79 significant health impacts than exposure to unmixed BB or urban emissions.

80 To be able to accurately predict and assess the impact of BB on human health, air quality and
81 climate, models must be able to realistically simulate the chemical and microphysical processes
82 that occur in a plume as well as plume transport and dispersion. In the case of BB plumes close
83 to an urban centre or other sensitive receptor, models can be used to mitigate risks on
84 community by forecasting where and when a BB plume will impact, the concentrations of toxic
85 trace gases and particles in the plume, and potential impact of the BB plume mixing with other
86 sources. Models also allow investigation of the contributions from BB and other sources on
87 observed air quality when multiple sources are contributing. Understanding the relative
88 importance of different sources is required when formulating policy decisions to improve air
89 quality.

90 Lagrangian parcel models are often used to investigate photochemical transformations in BB
91 plumes as they are transported and diluted downwind (Jost et al., 2003; Trentmann et al., 2005;
92 Mason et al., 2006; Alvarado and Prinn, 2009; Alvarado et al., 2015) while three-dimensional
93 (3D) Eulerian grid models have been used to investigate transport and dispersion of plumes,
94 plume age, as well as contributions from different sources. 3D Eulerian grid models vary from
95 fine spatial resolution on order of a few kilometers (Luhar et al., 2008; Keywood et al., 2015;
96 Alvarado et al., 2009; Lei et al., 2013) to a resolution of up to hundreds of kilometers in global
97 models (Arnold et al., 2015; Parrington et al., 2012).

98 Sensitivity studies have allowed the influence of different model components (emissions,
99 plume rise, transport, chemistry) on model output to be investigated. Such studies are
100 particularly important in formation of secondary species such as O₃ which have a non-linear
101 relationship with emissions. Studies have found that modelled O₃ concentration from BB
102 emissions is highly dependant on a range of factors including a) meteorology (plume transport
103 and dispersion) in global (Arnold et al., 2015) and high resolution (Lei et al., 2013) Eulerian
104 grid models, b) absolute emissions/biomass burned (Pacifico et al., 2015; Parrington et al.,
105 2012), c) model grid size resulting in different degrees of plume dilution (Alvarado et al.,

106 2009), and oxidative photochemical reaction mechanisms in Lagrangian parcel models (Mason
107 et al., 2006).

108 Broadly speaking, models used for simulating BB plumes comprise a) description of the
109 emissions source b) a determination of plume rise c) treatment of the vertical transport and
110 dispersion and d) a mechanism for simulating chemical transformations in the plume (Goodrick
111 et al., 2013). There are challenges associated with accurately representing each of these
112 components in BB modelling. The description of emissions source includes a spatial and
113 temporal description of the area burnt, the fuel load, combustion completeness, and trace gas
114 and aerosol emission factors (mass of species emitted per mass of fuel burned).- The area
115 burned is often determined by a combination of hotspot and fire scar data, determined from
116 retrievals from satellite (Kaiser et al., 2012; Reid et al., 2009; Giglio et al., 2013). Cloud cover
117 may lead to difficulties in obtaining area burnt data, while scars from small fires may be
118 difficult to discern against complex terrain, and low intensity fires may not correspond with a
119 detectable hotspot (Meyer et al., 2008). Emission factors are determined experimentally either
120 by field or laboratory measurements, and are typically grouped by biome type. In some regions,
121 such as SE Australia, biomes have been sparsely characterised (Lawson et al., 2015).
122 Furthermore, models use biome-averaged EF which do not account for complex intra-biome
123 variation in EF as a result of temporal and spatial differences in environmental variables. This
124 includes factors such as impact of vegetation structure, monthly average rainfall (van Leeuwen
125 and van der Werf, 2011) and the influence of short term rainfall events (Lawson et al., 2015).
126 For example, EFs have been shown to vary significantly with fuel moisture which can vary
127 seasonally (Korontzi et al., 2003; Urbanski, 2013). There may be significant spatial variability
128 in emission factors within a biome (Castellanos et al., 2014); taken along with temporal
129 variability, this has been shown to have a large impact on simulated concentrations of BB
130 species in global-scale modelling (van Leeuwen et al., 2013).

131 Finally, the very complex mixture of trace gases and aerosols in BB plumes creates analytical
132 challenges in quantifying EF, especially for semi and low volatility organics which are
133 challenging to measure and identify but contribute significantly to secondary aerosol formation
134 and photochemistry within the plume (Alvarado and Prinn, 2009; Alvarado et al., 2015; Ortega
135 et al., 2013).

136 Plume rise is a description of how high the buoyant smoke plume rises above the fire, and
137 consequently the initial vertical distribution of trace gases and aerosols in the plume (Freitas
138 et al., 2007). This is still a large area of uncertainty in BB models, with a generalised plume

139 rise approach typically used which may include either homogenous mixing, prescribed
140 fractions of emissions distributed according to mixing height, use of parametisations, and
141 finally plume rise calculated according to atmospheric dynamics. A key driver of this
142 uncertainty is the complexity of fire behaviour resulting in high spatial and temporal
143 variability of pollutant and heat release, which drives variability in plume rise behaviour,
144 such as multiple updraft cores (Goodrick et al., 2013).

145 Transport and dilution in models is driven by meteorology, particularly wind speed and
146 direction, wind shear and atmospheric stability. Meteorology has a large impact on the ability
147 of models to simulate the timing and magnitude and even composition of BB plume impacts in
148 both local and regional scale models (Lei et al., 2013; Luhar et al., 2008; Arnold et al., 2015).
149 For example, too-high wind speeds can lead to modelled pollutant levels which are lower than
150 observed (e.g. Lei et al., 2013) while small deviations in wind direction lead to large
151 concentration differences between modelled and observed, particularly when modelling
152 emissions of multiple spatially diverse fires (Luhar et al., 2008). Dilution of BB emissions in
153 large grid boxes in global models may also lead to discrepancies between modelled and
154 observed NO_x , O_3 and aerosols (Alvarado et al., 2009).

155 Finally, models use a variety of gas-phase and aerosol-phase physical and chemical schemes,
156 which vary in their ability to accurately represent chemical transformations, including
157 formation of O_3 and organic aerosol (Alvarado and Prinn, 2009; Alvarado et al., 2015).
158 Validating and constraining chemical transformations in models requires high quality, high
159 time resolution BB observations of a wide range of trace gas and aerosol species, including
160 important but infrequently measured species such as OH and semi volatile and low volatility
161 NMOC. Field observations, whilst often temporally and spatially scarce, are particularly
162 valuable because the processes and products of BB plume processing are dependent on long
163 range transport, cloud processing, varying meteorological conditions and heterogeneous
164 reactions.

165 In this work we test the ability of CSIRO's high resolution 3D Eulerian grid chemical transport
166 model (CTM) to reproduce BB plume observations of the Robbins Island fire reported in
167 Lawson et al., (2015) with a focus on CO, BC and O_3 . We undertake sensitivity studies using
168 varying emission factors associated with a low, medium and high Modified Combustion
169 Efficiency (MCE), which in turn changes the NMOC / NO_x ratio, in contrast to other sensitivity
170 studies which typically ~~vary-scale emissions of all species linearly by a constant factor~~ (Pacifico
171 et al., 2015; Lei et al., 2013). We also test sensitivity to meteorology by coupling the CTM

172 with two different meteorological models, TAPM and CCAM. The fire and fixed observation
173 site (Cape Grim) were only 20 km apart, and so simulation of the plume strikes is a stringent
174 test of TAPM and CCAM's ability to reproduce windspeed and direction. Plume rise and
175 chemical mechanism are held constant. Finally, we use TAPM-CTM to separate the
176 contribution of the Robbins Island fire emissions and urban emissions to the observed O₃
177 enhancements at Cape Grim reported in Lawson et al., (2015), and to determine the age of the
178 O₃-enhanced air parcels.

179 **2 Methods**

180 **2.1 Fire and measurement details**

181 Details of the fire and measurements are given in Lawson et al (2015). Briefly, biomass burning
182 (BB) plumes were measured at the Cape Grim Baseline Air Pollution Station during the 2006
183 Precursors to Particles campaign, when emissions from a fire on nearby Robbins Island
184 impacted the station. Fire burned through native heathland and pasture grass on Robbins Island
185 some 20 km to the east of Cape Grim for two weeks in February 2006. On two occasions an
186 easterly wind advected the BB plume directly to the Cape Grim Station. The first plume strike
187 (BB1) occurred from 02:00 – 06:00 (Australian Eastern Standard Time - AEST) on the 16th
188 February, with light easterly winds of 3 m s⁻¹ and temperature of 13 °C and RH of 96 %. The
189 second, more prolonged plume strike (BB2) occurred from 23:00 on 23rd February to 05:00
190 on the 25th February, with strong easterly winds ranging from 10-16 m s⁻¹, temperatures of 16-
191 22 °C and RH in the range of 75-95 %. Under a northerly wind direction, urban air from the
192 city of Melbourne (population 4.2 million) some 300 km away is transported across the ocean
193 (Bass Strait) to Cape Grim.

194 A wide variety of trace gas and aerosol measurements were made during the fire event (Lawson
195 et al., 2015). In this work, measurements of black carbon (BC), carbon monoxide (CO) and
196 ozone (O₃) are compared with model output. BC measurements were made using an
197 aethelometer (Gras, 2007), CO measurements were made using an AGAGE gas
198 chromatography system with a multi-detector (Krummel et al., 2007) and O₃ measurements
199 were made using a TECO analyser (Galbally et al., 2007). For further details see Lawson et al.,
200 (2015).

201 **2.2 Chemical transport models**

202 Simulations were undertaken with CSIRO's chemical transport model (CTM), coupled offline
203 with two meteorological models (see below). The CSIRO CTM is a three-dimensional Eulerian
204 chemical transport model with the capability of modelling the emission, transport, chemical
205 transformation, wet and dry deposition of a coupled gas and aerosol phase atmospheric system.
206 The CTM was initially developed for air quality forecasting (Cope et al., 2004) and has had
207 extensive use with shipping emission simulations (Broome et al., 2016), urban air quality (Cope
208 et al., 2014; Galbally et al., 2008), biogenic (Emmerson et al., 2016) and biomass burning
209 studies (Keywood et al., 2015; Meyer et al., 2008; Luhar et al., 2008).

210 The chemical transformation of gas-phase species was modelled using an extended version of
211 the Carbon Bond 5 mechanism (Sarwar et al., 2008) with updated toluene chemistry (Sarwar
212 et al., 2011). The mechanism was also extended to include the gas phase precursors for
213 secondary (gas and aqueous phase) inorganic and organic aerosols. Secondary inorganic
214 aerosols were assumed to exist in thermodynamic equilibrium with gas phase precursors and
215 were modelled using the ISORROPIA-II model (Fountoukis and Nenes, 2007). Secondary
216 organic aerosol (SOA) was modelled using the Volatility Basis Set (VBS) approach (Donahue
217 et al., 2006). The VBS configuration is similar to that described in Tsimpidi et al., (2010). The
218 production of S-VI in cloud water was modelled using the approach described in Seinfeld and
219 Pandis (1998). The boundary concentrations in the models for different wind directions were
220 informed by Cape Grim observations of atmospheric constituents during non BB periods
221 (Lawson et al., 2015). In this work the modelled elemental carbon (EC) output was considered
222 equivalent to the BC measured with aethalometer at Cape Grim.

223 Horizontal diffusion is simulated according to equations detailed in Cope et al (2009) according
224 to principles of Smagorinsky et al., (1963) and Hess (1989). Vertical diffusion is simulated
225 according to equations detailed in Cope et al., (2009) according to principles of Draxler and
226 Hess (1997). Horizontal and vertical advection uses the approach of Walcek et al., (2000).

227 **2.2.1 Meteorological models**

228 Prognostic meteorological modelling was used for the prediction of meteorological fields
229 including wind velocity, temperature, water vapour mixing ratio and clouds, radiation and
230 turbulence. The meteorological fields force key components of the emissions and the chemical
231 transport model. Two meteorological models were used in this work. CSIRO's (The) Air
232 Pollution Model (TAPM) (Hurley, 2008b), a limited area, nest-able, three-dimensional

233 Eulerian numerical weather and air quality prediction system, and CSIRO's Conformal Cubic
234 Atmospheric Model (CCAM) a global stretched grid atmospheric simulation model
235 (McGregor, (2015) and references therein). The models represent two unique (and
236 independent) approaches for generating the meteorological fields required by the chemical
237 transport model.

238 For CCAM, 20 km spaced simulations over Australia were used by the CTM (with the same
239 grid spacing) to model large scale processes on the continent including the emission and
240 transport of windblown dust, sea salt aerosol and smoke from wildfires. Note that the governing
241 equations for TAPM do not enable this model to simulate spatial scales greater than 1000 km
242 in the horizontal and thus only the CCAM meteorology was available for the continental-scale
243 simulations. TAPM and CCAM 12 km spaced simulations were then used to model the
244 transport of the Melbourne plume to Cape Grim by the CTM (at 12 km grid spacing) with
245 boundary conditions provided by the continental simulation. Nested grid simulations by the
246 CTM at 3 km and 1 km grid spacing utilised TAPM and CCAM meteorology simulated at
247 matching grid spacing. The 1 km spaced meteorological fields were also used to drive a 400 m
248 spaced CTM domain which encompassed Robbin's Island and Cape Grim. This domain was
249 included in the nested grid system because we wanted to better numerically resolve the spatial
250 extent of the fire and the process of plume advection between Robbin's Island and Cape Grim.

251 Figure 1 shows the five nested computational domains used in TAPM-CTM and CCAM-CTM.

252 In this work the CTM coupled with CCAM meteorological model is referred to as CTM-
253 CCAM, while the CTM coupled with the TAPM meteorological model is referred to as TAPM-
254 CTM.

255 2.2.2 Emission inventories

256 **Anthropogenic emissions**

257 Anthropogenic emissions for Victoria were based on the work of Delaney et al., (2011). No
258 anthropogenic emissions were included for Tasmania. The north-west section of Tasmania has
259 limited habitation and is mainly farmland, and so the influence of Tasmanian anthropogenic
260 emissions on Cape Grim are expected to be negligible.

261 **Natural and Biogenic emissions**

262 The modelling framework includes methodologies for estimating emissions of sea salt aerosol
263 (Gong, 2003) emissions of windblown dust (Lu and Shao, 1999); gaseous and aerosol

264 emissions from managed and unmanaged wild fires (Meyer et al., 2008); emissions of NMOC
265 from vegetation (Azzi et al., 2012) and emissions of nitric oxide and ammonia from vegetation
266 and soils. Emissions from all but the wildfires are calculated inline in the CTM at each time
267 step using the current meteorological fields. There were no other major fires burning in Victoria
268 and Tasmania during the study period.

269 **Emissions – Robbins Island fire**

270 The area burnt by the fire was determined from hotspots from the Sentinel product
271 (Geosciences Australia) which were derived from MODIS imagery. The hotspots were
272 buffered to give polygon spots at a resolution of 400ha spot⁻¹, then merged into a single
273 polygon for each fire day (Meyer et al., 2008). ~~The fire burnt 2000 ha over the two week~~
274 period, and the direction of fire spread was unknown. As such, the fire scar was divided up
275 into 250m grids and the hourly areas burnt calculated using a normalised version of the
276 Macarthur Fire Danger Index (FDI) (Meyer et al., 2008). The models assumed that an equal
277 proportion of each grid burned simultaneously over the two week period. The fuel density used
278 was estimated to be 18.7 t C ha⁻¹, based on mean mass loads of coarse and fine fuels taken from
279 the biogeochemical production model (VAST 1.2, Barrett 2002) and converted into carbon
280 mass (Meyer et al., 2008).

281 The hourly diurnal emissions of all gases and particles from the fire were calculated using the
282 FDI in which the presence of strong winds will result in faster fire spread and enhanced
283 emissions, compared to periods of lower wind speeds. The effect of wind speed on the fire
284 behaviour and emissions is particularly important during the second BB event in which the
285 winds ranged from 10 to 15 m s⁻¹. This is evident from Figure 2 where hourly emission profiles
286 based on an average diurnal FDI calculated by Meyer et al., (2008) (which peaks early
287 afternoon) is compared with profiles based on hourly FDI generated by TAPM and CCAM
288 meteorology. It can be seen that the use of the dynamic FDI approach during the BB2 period
289 increases the Base emissions by 70% for TAPM meteorology and by 45% for the CCAM
290 meteorology. It is also notable that the use of the dynamic approach with TAPM meteorology
291 leads to the peak emissions occurring overnight on the 24th Feb which is when the Base
292 emissions are at a minimum.

293 ~~Savanna category EF were used as base case EFs in this work from Andreae and Merlet (2001).~~

294 Three different sets of fire emission factors, corresponding to low, medium and high MCE
295 were used to test the sensitivity of the models, where $MCE = \Delta CO_2 / \Delta CO + \Delta CO_2$ (Ferek et

296 al., 1998). We used published EF of CO and CO₂ from temperate forests (Akagi et al., 2011),
297 to calculate a typical range of MCEs for temperate fires, including an average (best estimate)
298 of 0.92, a lower (0.89) and upper estimate (0.95). Fires with MCEs of approximately 0.90
299 consume biomass with approximately equal amounts of smouldering and flaming, while MCEs
300 of 0.99 indicate complete flaming combustion (Akagi et al., 2011). Therefore the calculated
301 range of MCEs (0.89 - 0.95) correspond to fires in which both smouldering and flaming is
302 occurring, with a tendency for more flaming combustion in the upper estimate (0.95) compared
303 to a tendency of more smouldering in the lower estimate (0.89).

304 In previous smoke modelling work, CCAM-CTM and TAPM-CTM used savannah EF from
305 Andreae and Merlet (2001). However, as Robbins Island is in a temperate region, the Andreae
306 and Merlet (2001) savannah EF used in the models were adjusted to reflect temperate EF based
307 on the following methodology. Minimum, mean and maximum CO EF for temperate forests
308 from Agaki et al., (2011) were used for lower ~~(0.89)~~, best estimate ~~(0.92)~~ and upper MCE
309 ~~(0.95)~~. For all other species, savannah EF (corresponding to MCE 0.94) were adjusted to EF
310 for the lower, best estimate and upper MCEs=0.89, 0.92 and 0.95 using published relationships
311 between MCE and EF (Meyer et al., 2012; Yokelson et al., 2007; Yokelson et al., 2003;
312 Yokelson et al., 2011).

313 For example to adjust the Andreae and Merlet (2001) savannah EF (corresponding to an MCE
314 of 0.94) to our temperate 'best estimate' EF (corresponding to MCE of 0.92) the Andreae and
315 Merlet (2001) NO EF was reduced by 30%, the NMOC EFs were increased by 30%, the BC
316 EF was reduced by 30% and the OC EF was increased by 20%. Table 1 gives emission factors
317 for the original savannah EF (Andreae and Merlet, 2001) and the adjusted EF used in this work.
318 The NO_x/NMOC ratios used are also shown, and vary by a factor of 3 between the low and
319 high MCE scenarios, mainly driven by the variability in NO emissions with MCE. The EF
320 calculated from observations for this fire are shown for comparison (Lawson et al., 2015).

321 We recognise calculating EF in this way is approximate, however the purpose of including a
322 range of EF was to explore the model's sensitivity to EF. While EFs were calculated for the
323 Robbins Island fire for several species (Lawson et al., 2015), these are only available for a
324 subset of species required by the CB05 chemical mechanism. The adjustment of the Andreae
325 and Merlet (2001) Savannah EF to a lower MCE (0.89) resulted in good ($\pm 20\%$) agreement
326 with the calculated EF for CO, BC and several NMOC from Lawson et al., (2015), in which
327 the MCE was calculated as 0.88. This provides confidence in using published relationships
328 between MCE and EF to estimate EF in this work.

329 With respect to plume rise, the Robbin's Island fire was a relatively low energy burn (Lawson
330 et al., 2015), and as noted by Paugam et al., (2016) the smoke from such fires is largely
331 contained within the planetary boundary layer (PBL). Given that ground-based images of the
332 Robbin's Island smoke plume support this hypothesis, in this work we adopted a simple
333 approach of mixing the emitted smoke uniformly into the model's layers contained within the
334 PBL. The plume was well mixed between the maximum of the PBL height and 200 m above
335 the ground, with the latter included to account for some vertical mixing of the buoyant smoke
336 plume even under conditions of very low PBL height. The high wind speeds particularly during
337 the second BB event, also suggest that the plume was not likely to be sufficiently buoyant to
338 penetrate the PBL.

339

340 **3 Results and Discussion**

341 **3.1 Modelling Sensitivity Study**

342 The ability of the models to reproduce the two plume strikes (BB1 and BB2, described in
343 Lawson et al (2015)) was tested. The period examined was the 13 February 2006 to the 28
344 February 2006. The sensitivity of the models to meteorology, emission factors and spatial
345 variability was also investigated and is discussed below. Observation and model data shown
346 are hourly averages. Table 2 summarizes the main findings of the model sensitivity study. A
347 MODIS Truecolour Aqua image of the Robbins Island fire plume is shown in Figure 3 from
348 23 February 2006, with the modelled plume during the same period.

349 **3.1.1 Sensitivity of modelled BB species to meteorology**

350 Qualitative and quantitative assessment of model performance for meteorological parameters
351 were undertaken for both TAPM and CCAM. Hourly observed and modelled winds,
352 temperature, humidity and PBL are compared and discussed in the Supplementary section
353 (Figures S2-S8). Briefly, both TAPM and CCAM demonstrated reasonable skill in modelling
354 the meteorological conditions, with the TAPM simulations slightly better than the CCAM with
355 respect to the low level wind, temperatures and relative humidity and CCAM simulations
356 slightly better in terms of PBL height.

357 **Primary species- CO and BC**

358 Figure 4 and Figure 5 show concentration isopleths for BC generated by TAPM-CTM and
359 CCAM-CTM for BB1 and BB2 respectively. The simulated and observed time series
360 concentrations of CO and BC for the two different models (TAPM-CTM and CCAM-CTM)
361 and for 3 different sets of EF (discussed in Section 3.1.2) are shown in Figure 6. TAPM-CTM
362 and CCAM-CTM both reproduce the observed plume strikes (BB1 and BB2). The impact of
363 meteorology on the plume strike timing and duration is discussed below.

364 Both models overestimate the duration of BB1 and are a few hours out in the timing of the
365 plume strike. TAPM-CTM predicts the timing of BB1 is 3 hours later than occurred (BC data)
366 and predicts that BB1 persists for 12 hours (observed duration 5 hours). CCAM-CTM predicts
367 that BB1 occurs 12 hours prior to the observed plume strike and predicts that the plume
368 intermittently sweeps across Cape Grim for up to 36 hours (Figure 4). Both models indicate
369 that the plume is narrow and meandering.

370 Both models overestimate the duration of BB2 and simulate the plume strike occurring earlier
371 than observed. TAPM-CTM predicts BB2 is 26 hours earlier than observed and that BB2
372 persists for 50 hours (observed duration 29 hours). CCAM-CTM predicts BB2 is 26 hours
373 earlier than observed and that BB2 persists for 57 hours. It should be noted that there is a brief
374 observed enhancement of BB species which correspond with the beginning of the modelled
375 BB2 plume strike, some 24 hours prior to the prolonged observed event. This was likely due
376 to the edge of the plume impacting the station briefly.

377

378 In both observed BB1 and BB2 the plume strike at Cape Grim occurred just prior to a wind
379 direction change from easterly (fire direction), to south-westerly. The timing of the wind
380 direction change in the models is therefore crucial to correctly predicting plume strike time and
381 duration. In BB1 CCAM predicts an earlier wind direction change with higher windspeeds
382 which advects the plume directly over Cape Grim while TAPM predicts a later wind change,
383 lower windspeeds and advection of only the edge of the plume over Cape Grim. The higher
384 concentrations CO and BC in BB1 by CCAM-CTM is are likely due to the direct advection of
385 the plume over the site compared to only the plume edge in TAPM-CTM.

386 In BB2, both TAPM-CTM and CCAM-CTM predict direct strikes of the Robbin's Island
387 smoke plume on Cape Grim, because the wind direction is modelled to be predominantly
388 easterly for the duration of the event (Figure 5 Fig-S18). Both models simulate some backing
389 and veering of the wind direction for the duration of BB2 due to gravity waves processes which

390 lead to intermittent strikes on Cape Grim as the Robbin's Island smoke plume sweeps to the
391 north and south of Cape Grim. The gravity wave oscillations are more pronounced in CCAM-
392 CTM than TAPM-CTM (and thus the plume strikes are more pronounced from the former) due
393 to differences in how the models are coupled to large scale synoptic forcing. The event is
394 eventually curtailed by the passage of a south-westerly change.

395 Figure 5~~Fig. S18~~ shows that TAPM-CTM predicts the onset of the change to occur about six
396 hours ahead of the observed change and thus the BB2 event ends too early for this
397 meteorological simulation. CCAM-CTM models the south-westerly change to occur one hour
398 after the observed, leading to the modelled BB2 event extending beyond the observed duration
399 for this meteorological simulation.

400 Differences in the magnitude of the modelled CO and BC peaks for TAPM-CTM and CCAM-
401 CTM have two principal cause: a), the coupling of the smoke emissions to the TAPM and
402 CCAM meteorology via the FDI scaling leads to approximately 20% higher emissions in the
403 case of the TAPM-CTM simulations; b), the CCAM wind speeds are 20-50% higher than the
404 TAPM wind speeds during BB2, which in combination with the emission differences, leads to
405 TAPM-CTM generating near-surface smoke concentrations which are up to 80% higher than
406 CCAM-CTM. Mixing depth can also play an important role in plume dispersion, however the
407 PBL heights generated by both models are similar and generally low during BB2 due to the
408 easterly wind direction and the mainly maritime upwind fetch.

409 **Secondary species – O₃**

410 Figure 6 e-f shows the simulated and actual O₃ concentration time series for TAPM-CTM and
411 CCAM-CTM for 3 different sets of EF (discussed in Section 3.1.2). The two observed O₃ peaks
412 which followed BB1 and BB2 can clearly be seen in the time series of observations. Figure
413 ~~7Figure 7~~ shows the TAPM-CTM and CCAM-CTM concentration isopleths of O₃
414 enhancement downwind of the fire during BB1 at 11:00 and 13:00 on the 16 February.

415 Again the simulated meteorology has a major impact on the ability of the models to reproduce
416 the magnitude and timing of the observed O₃ peaks. TAPM-CTM reproduces the major O₃ peak
417 observed following BB2, and captures part of the O₃ peak following BB1. For the peak
418 following BB1 it under predicts the peak duration and fails to capture the subsequent observed
419 peaks on the 19th and 19th February. TAPM-CTM also shows 2 additional O₃ peaks about
420 24 hours prior to the BB1 and BB2 peaks respectively, which were not observed. The
421 magnitude of these additional peaks shows a strong dependency on the EF suggesting an

422 influence of fire emissions. This is discussed further below and in Section 3.2.1. Compared to
423 TAPM-CTM, CCAM-CTM predicts fewer distinct peaks of ozone above the background
424 (where background is 15-17 ppb) throughout the entire period. Both TAPM-CTM and CCAM-
425 CTM show depletion of O₃ below background levels which was not observed, and this is
426 discussed further in Section 3.1.2.

427 Figure 7 shows that there are differences in wind fields between TAPM-CTM and
428 CCAM-CTM as well as different simulated concentrations of O₃ generated from the fire. This
429 is discussed further in Section 3.1.2. To summarise, the impact of using two different
430 meteorological models for a primary species such as BC was to vary the modelled time of
431 impact of the BB1 plume strike by up to 15 hours (CCAM-CTM -12 and TAPM-CTM +3
432 hours, where actual plume strike time = 0 hours) and to vary the plume duration between 12
433 and 36 hours (actual duration 5 hours). For BB2, different meteorological models predicted the
434 same impact time (TAPM-CTM and CCAM-CTM both -26 hours where actual plume strike
435 time = 0 hours) and to vary the plume duration between 47 and 60 hours (actual duration 29
436 hours).

437 For O₃, the use of different meteorological models lead to one model (TAPM-CTM)
438 reproducing both observed peaks plus two additional peaks, while the other model (CCAM-
439 CTM) captured only one defined O₃ peak over the time series of 2 weeks.

440 3.1.2 Sensitivity of modelled BB species to Emission Factors

441 **Primary species – CO and BC**

442 Figure 6 a-d shows the simulated and observed concentrations of BC and CO for MCE=0.89,
443 MCE=0.92 and MCE=0.95 (see Section 2.2.2). Because CO has a negative relationship with
444 MCE, and BC has a positive relationship with MCE, the modelled BC concentrations are
445 highest for model runs using the highest MCE, while the modelled CO concentrations are
446 highest for model runs using the lowest MCE (Figure 6).

447 Changing the EF from low to high MCE varies the modelled BC concentrations during BB1
448 and BB2 by a factor of ~3 for BC and a factor of ~2 for CO, and increases the EF ratio of
449 BC/CO by a factor of ~6, in proportion to the difference in EF input to the models.

450 Quantile-quantile plots of observed and modelled ratios of BC/CO during BB1 and BB2 for
451 the different EF scenarios are shown in Figure 8. The use of BC/CO ratios were used
452 to minimise uncertainty resulting from errors in modelling transport, dilution (and mixing

453 height), thus enabling a focus on the impact of EF variability. A period incorporating both the
454 modelled and observed BB1 and BB2 was used for the analysis. The TAPM-CTM simulation
455 with MCE=0.89 performed best with greater than 60% of the model percentiles falling within
456 a factor of two of the observed. The CCAM-CTM simulation with MCE = 0.89 was the second
457 best performer with 50% of the modelled percentiles falling within a factor of two of the
458 observed. Overestimates of the EC/CO ratio by up to a factor of 8 occur for some percentiles
459 for the MCE=0.95 scenarios, while the scenarios with no fire significantly underestimated the
460 observed ratio. Plots of mean fractional bias and mean fractional error (Fig. S121 and S123)
461 show that TAPM-CTM simulation with MCE=0.89 has the smallest bias and error, followed
462 by the CCAM-CTM simulation with MCE=0.89. As discussed previously there is uncertainty
463 in the derivation of EF as a function of MCE, as these were based on relationships from a small
464 number of studies. Nevertheless, the percentile, bias and error analysis indicates that using
465 emission factors corresponding to an MCE of 0.89 gives the best agreement with the
466 observations for the BC/CO ratio. This is in agreement with the calculated MCE of 0.88 for
467 this fire (Lawson et al., 2015)

468

469

470 **Secondary species - O₃**

471 For secondary species such as O₃ (Figure 6e-f), the relationship between EF precursor gases
472 and model output is more complex than for primary species such as CO and BC, because the
473 balance between O₃ formation and destruction is dependent on the degree of dilution of the BB
474 emissions and also factors such as the NMOC composition and the NMOC/NO_x ratio.

475 TAPM-CTM (Figure 6e) reproduces the magnitude of both observed peaks following BB1
476 and BB2 (BB1 max observed = 33 ppb, modelled = 31 ppb, BB2 max observed = 34 ppb,
477 modelled = 30ppb). Interestingly the magnitude of O₃ for these two peaks is the same for
478 different EF inputs of O₃ precursors from the Robbins Island fire, suggesting that the BB
479 emissions are not responsible for these enhancements as demonstrated in Section 3.2. In
480 contrast, the two additional peaks modelled but not seen in the observations are heavily
481 dependent on the input EF. For the first additional modelled peak which was predicted at the
482 time of BB1 observations on the 16th February, all EF scenarios result in an O₃ peak, with the
483 MCE=0.92 model scenario resulting in highest predicted O₃. For the second additional
484 modelled peak just prior to the BB2 observations on the 23rd February, only the MCE=0.89

485 scenario results in a net O₃ production, while MCE=0.92 and MCE=0.95 scenarios lead to net
486 O₃ destruction.

487 This differing response to EF for the TAPM-CTM runs suggests the importance of the NO EF
488 on O₃ production in BB plumes. Unfortunately there were no oxides of nitrogen measurements
489 made during the fire to test the models. For the first simulated additional peak prior to BB1,
490 while the medium NO EF (MCE=0.92) resulted in the highest O₃ peak (with corresponding
491 NO of 3.7 ppb, NO₂ 4.5 ppb) the lower NO EF in the 0.89 MCE run perhaps indicates
492 insufficient NO was present to drive O₃ production (corresponding NO 0.5 ppb, NO₂ 1.5 ppb),
493 which is in line with studies which have shown that BB plumes are generally NO_x limited
494 (Akagi et al., 2013; Jaffe and Wigder, 2012; Wigder et al., 2013). Conversely the highest input
495 NO EF (MCE=0.95) lead to net destruction of O₃ (NO 9 ppb, NO₂ 7 ppb), which is due to
496 titration of O₃ with the larger amounts of NO emitted from the fire in these runs as indicated
497 by excess NO (NO/NO₂ ratio > 1) at Cape Grim (where NO has a positive relationship with
498 MCE). For the second additional peak prior to BB2, only the lowest NO EF run (MCE=0.89)
499 resulted in net production of O₃ (NO 1.5 ppb NO₂ 2.6 ppb) in the medium and high MCE runs
500 the background O₃ concentration is completely titrated (0 ppb) with NO concentrations of 10
501 and 20 ppb and NO/NO₂ ratios of 1.3 and 2.6 respectively.

502 In contrast, the CCAM-CTM model (Figure 6f) simulations reproduce only the first observed
503 O₃ peak associated with BB1 (modelled = 27 ppb, measured = 34 ppb). This modelled O₃ peak
504 does not show an influence of MCE on O₃ concentration, in agreement with TAPM, again
505 suggesting no influence from fire emissions as later demonstrated in Section 3.2. The CCAM
506 model runs also show significant titration of O₃ during BB1 and BB2 for the medium and high
507 MCE model runs, with ~24 and ~48 hours of significant O₃ depletion below background
508 concentrations being modelled for each event, which was not observed

509 Quantile-quantile plots of modelled and observed concentrations of O₃ for all EF scenarios are
510 shown in Figure 9 ~~Figure 8~~ Fig. S14 and S135. Model performance was assessed for both the
511 BB and the background periods in order to test the ability of the models to reproduce O₃ from
512 both the fire and other sources, including urban sources. The modelled O₃ concentrations from
513 the TAPM-CTM simulation with MCE=0.89 are close to the 1:1 line with observations for all
514 of the sampled percentiles, and demonstrates that this scenario is in best agreement with
515 observations, and as stated previously, in agreement with the calculated MCE of 0.88 for BB2
516 (Lawson et al., 2015). Ozone titration in the MCE=0.92 and MCE=0.95 scenarios, which was
517 not observed, is visible as a significant deviation from the 1:1 line in Figure 9 Fig. S14. With

518 the exception of these titration events, all of the sampled model concentration percentiles fall
519 well within a factor of two of the observations. Plots of mean fractional error and mean
520 fractional bias (Figs S146 and S157) show that the error and bias are very low for all runs and
521 fall within performance guidelines.

522 The different EF scenarios presented here suggest that varying model EF has a major impact
523 on whether the models simulate production or destruction of O₃, particularly important at a
524 receptor site in close proximity to the BB emissions. In the previous work (Lawson et al., 2015),
525 the MCE for the first 10 hours of BB2 was calculated as 0.88, however later in BB2, a rainfall
526 event led to changes in the NMOC/CO and BC/CO ratios. This suggests that during the course
527 of BB2 the MCE decreased and thus EFs changed. As such, the used of fixed BB EF in this
528 work and in other models, may lead to incorrect prediction of important species such as O₃.

529 3.1.3 Sensitivity of modelled concentrations to spatial variability

530 The near-field proximity of the Robbins Island fire (20 km) to Cape Grim, the narrowness of
531 the BB plume and the spatial complexity of the modelled wind fields around north Tasmania
532 are likely to result in strong heterogeneity in the modelled concentrations surrounding Cape
533 Grim. We investigated how much model spatial gradients vary by sampling TAPM-CTM
534 output with MCE=0.89 at 4 grid points sited 1 km to the north, east, south and west of Cape
535 Grim.

536 **Primary species - CO**

537 Figure 10a shows a time series of the modelled CO output of the difference between Cape
538 Grim and each grid point 1km either side.

539 Where plotted CO concentration is other location [CO] (N,S,E,W) –Cape Grim [CO].

540 The figure clearly shows that there are some large differences in the modelled concentrations
541 of CO between grid points for both BB1 and BB2. Particularly large differences were seen for
542 BB2 with the north gridpoint modelled concentrations in BB2 over 500 ppb lower than at Cape
543 Grim grid point, while at the Southerly grid point the modelled CO was up to 350 ppb higher.
544 Smaller differences of up to 250 ppb between the east and Cape Grim grid points were observed
545 for BB1. This indicates the plume from the fire was narrow and had a highly variably impact
546 on the area immediately surrounding Cape Grim.

547 Figure 10b shows the observed cumulative concentration of CO over the 29 hour
548 duration of BB2 at Cape Grim, as well as the modelled cumulative concentration at Cape Grim

549 and at the four gridpoints either side. This figure shows both the variability in concentration
550 with location, but also with time. TAPM-CTM's underestimation of the observed CO by is
551 visible by hour 20. TAPM-CTM begins to show differences in modelled cumulative CO
552 concentrations between the 5 gridpoints (including Cape Grim) by hour 10. At the end of BB2
553 TAPM-CTM predicts that there are differences of 5 - 30% between the cumulative modelled
554 CO concentration at Cape Grim and the gridpoints to the north, east, south and west. his
555 variability modelled between sites which are closely located highlights the challenges with
556 modelling the impact of a near field fire at a fixed single point location. This also highlights
557 the high spatial variability which may be missed in similar situations by using a coarser
558 resolution model which would dilute emissions in a larger gridbox.

559 **Ozone (O₃)**

560 Figure 10~~Figure 8c~~ shows a time series of the modelled O₃ output of the difference between
561 Cape Grim and each gridpoint 1km either side, where plotted O₃ concentration is other location
562 [O₃] (N,S,E,W) – Cape Grim [O₃].

563 The modelled TAPM-CTM concentrations are very similar at all grid points when BB
564 emissions are not impacting. The variability increases at the time of BB1 and BB2, with
565 differences mostly within 2-3 ppb, but up to 15 and 10 ppb at east and west sites for BB1. This
566 largest difference corresponds to the additional modelled O₃ peak which was not observed
567 which showed strong dependency on EF (see Section 3.1.2), and provides further evidence that
568 local BB emissions are driving this enhancement.

569 The TAPM-CTM output for O₃ for BB1(Figure 7~~Figure 7~~) shows O₃ enhancement downwind
570 of the fire at 11:00 and 13:00 on the 16 February. The very localised and narrow O₃ plume is
571 dispersed by the light (2 m s⁻¹) and variable winds, and Cape Grim is on the edge of the O₃
572 plume for much of this period, explaining the high variability seen in Figure 6c.

573 In summary there is a large amount of spatial variability in TAPM-CTM for primary species
574 such as CO during the BB events, with differences of > 500 ppb in grid points 1 km apart. This
575 is due to the close proximity of the fire to the observation site and narrow plume non-stationary
576 meteorology. For O₃, there is up to 15 ppb difference between grid points for a narrow O₃
577 plume which is formed downwind of the fire.

578 The highly localised nature of the primary and in some cases secondary species seen here
579 highlights the benefits of assessing spatial variability in situations with a close proximity point
580 source and a fixed receptor (measurement) site.

581 3.2 Exploring plume chemistry and contribution from different sources

582 3.2.1 Drivers of O₃ production

583 In previous work on the Robbins Island fire, it was noted that the increases in O₃ observed after
584 both BB1 and BB2 were correlated with increased concentration of HFC134a (Lawson et al.,
585 2015). This indicated that transport of photochemically processed air from urban areas to Cape
586 Grim was likely the main driver of the O₃ observed, rather than BB emissions (Lawson et al.,
587 2015). However, during BB1 in a calm sunny period with minimal urban influence, an increase
588 in O₃ was observed alongside a period of particle growth and elevated BC, suggesting possible
589 biomass burning influence. Normalised Excess Mixing Ratios (NEMR) observed during BB2
590 were also in the range of those observed elsewhere in young BB plumes (Lawson et al., 2015)
591 (where NEMR is an excess mixing ratio normalised to a non-reactive co-emitted tracer, in this
592 case CO, see Akagi et al., 2011).

593 To explore this further, TAPM-CTM was used to determine the degree to which the local fire
594 emissions, and urban emissions from mainland Australia, were driving the observed O₃
595 enhancements. The scenario with EF corresponding to MCE=0.89 was used, as discussed
596 previously

597 Figure 11 ~~Figure 9~~ shows the simulated ozone for all sources (With BB) and all sources
598 excluding the Robbins Island fire (No BB). There are two additional distinct ozone peaks in
599 the 'With BB' simulation (Figure 11 ~~Figure 9~~). These occurred during, or close to the plume
600 strikes, and are short lived (3 and 5 hour) events. These same two peaks showed a strong
601 dependence on model EF in Section 3.1.2. In contrast, the two peaks attributed to transport of
602 air from mainland Australia are of longer duration, and occur after the plume strikes.

603 Of the 2 modelled fire-derived O₃ peaks, the first modelled peak (33 ppb) corresponds with a
604 small (21 ppb) observed peak during BB1 (Period B in Lawson et al., 2015), but the second
605 modelled fire-derived O₃ peak is not observed. As shown in Figure 7 ~~Figure 7~~ and discussed in
606 Section 3.1.3, according to TAPM-CTM the O₃ plumes generated from fire emissions were
607 narrow and showed a strong spatial variability. Given this, it is challenging for TAPM-CTM
608 to predict the exact timing and magnitude of these highly variable BB generated O₃ peaks
609 impacting Cape Grim. This is likely why there is good agreement in timing and magnitude
610 between model and observations for the large scale, spatially homogeneous O₃ plumes
611 transported from mainland Australia, but a lesser agreement for the locally formed, spatially
612 variable O₃ formed from local fire emissions.

613 In summary, TAPM-CTM suggests that the the two largest observed O₃ peaks following BB1
614 and BB2 were urban air transported from mainland Australia, and suggests some O₃ formation
615 was driven by emissions from the local fire event. TAPM-CTM captures the magnitude and
616 timing of the larger scale urban-derived peaks well, but is challenged by the timing and
617 magnitude of O₃ from local BB emissions.

618

619 3.2.2 Plume age

620 TAPM-CTM was used to estimate the physical age of air parcels reaching Cape Grim over the
621 two week period of the Robbins Island fire. The method is similar to the Eulerian effective
622 physical age of emissions metric, accounting for mixing and chemical decay from Finch et al
623 (2014) and has been described previously in Keywood et al., (2015). Briefly, two model
624 simulations were run for scenarios which included all sources of nitric oxide (NO) in Australia;
625 the first treated NO as an unreactive tracer, the second with NO decaying at a constant first
626 order rate. The relative fraction of the emitted NO molecules remaining after 96 hours was then
627 inverted to give a molar-weighted plume age. As urban emissions are a larger NO source than
628 BB, this approach would weight the age in the favour of the urban emissions if air masses from
629 these two sources were mixed. However as shown in Figure 11 ~~Figure 9~~, there are distinct
630 periods where BB or urban sources dominate. As there is little mixing of air from the two
631 sources, there are unlikely to be issues with the calculated age being weighted towards one
632 source. Figure 12 ~~Figure 10~~ shows a time series of the modelled NO tracer (decayed version),
633 modelled plume age (hours) and the observed O₃. Direct BB1 and BB2 plume strikes can be
634 clearly seen with increases in NO corresponding with a plume age of 0-2 hours. The plume
635 age then gradually increases over 24 hours in both cases, peaking at 15:00 on the 17th February
636 during BB1 (aged of plume 40 hours) and peaking at 17:00 on the 25th February during BB2
637 (age of plume 49 hours). The peak observed O₃ enhancements correspond with the simulated
638 plume age in both BB1 and BB2 (with an offset of 2 hours for BB1), and the observed HFC-
639 134a, suggesting that the plume which transported O₃ from Mebourne to Cape Grim was
640 approximately 2 days old. TAPM-CTM also simulates a smaller NO peak alongside the
641 maximum plume age, indicating transport of decayed NO from the mainland to Cape Grim.

642 As reported in Lawson et al., (2015), during BB2 NEMRs of $\Delta O_3/\Delta CO$ ranged from 0.001-
643 0.074, in agreement with O₃ enhancements observed in young BB plumes elsewhere (Yokelson
644 et al., 2003; Yokelson et al., 2009). However, the modelling reported here suggests that almost

645 all of the O₃ observed during BB2 was of urban, not BB origin. This suggests NEMRs should
646 not be used in isolation to identify the source of observed O₃ enhancements, and highlights the
647 value of utilising air mass back trajectories and modelling to interpret the source of O₃
648 enhancements where there are multiple emission sources.

649 **4 Summary and conclusions**

650 In this work we have used a unique set of opportunistic BB observations at Cape Grim Baseline
651 Air Pollution Station to test the ability of CSIRO's high resolution (400m grid cell) CTM to
652 reproduce primary (CO, BC) and secondary (O₃) BB species in challenging non-stationary,
653 inhomogeneous, and near field conditions. We tested the sensitivity of the CTM to three
654 different parameters (meteorology, MCE and spatial variability) while holding the plume rise
655 and the chemical mechanisms constant.

656 We found meteorology, EF and spatial variability have a large influence on the modelled output
657 mainly due to the close proximity of the fire to the receptor site (Cape Grim). The lower MCE
658 (MCE=0.89) TAPM-CTM model simulation provided the best agreement with the observed
659 concentrations, in agreement with the MCE calculated from observations of 0.88 (Lawson et
660 al., 2015). The changing EFs, in particular NO dependency on MCE, had a major influence on
661 the simulated O₃ concentrations, with a tendency of the models in some configurations to both
662 fail to simulate observed O₃ peaks, and to simulate complete titration of O₃ which was not
663 observed. As shown in the previous work (Lawson et al., 2015), minor rainfall events have the
664 potential to significantly alter EF due to changes in combustion processes. This work suggests
665 that varying model EF has a major impact on whether the models predict production or
666 destruction of O₃, particularly important at a receptor site in close proximity to the BB
667 emissions. Models which assume a fixed EF for O₃ precursor species in an environment with
668 temporally and spatially variable EF may therefore be challenged to correctly predict the
669 behaviour of important species such as O₃.

670 There were significant differences in model output between Cape Grim and grid points 1 km
671 away highlighting the narrowness of the plume and the challenge of predicting when the plume
672 would impact the station. This also highlights the high spatial variability which may be missed
673 in similar situations by using a coarser resolution model which would dilute emissions in a
674 larger gridbox.

675 TAPM-CTM was used to distinguish the influence of the two sources on the observed O₃
676 enhancements which followed BB1 and BB2. Transport of a 2 day old urban plume some

677 300km away from Melbourne was the main source of the O₃ enhancement observed at Cape
678 Grim over the two week period of the fire. Despite NEMRs of $\Delta\text{O}_3/\Delta\text{CO}$ during BB2 being
679 similar to that observed in young BB plumes elsewhere, this work suggests NEMRs should not
680 be used in isolation to identify the source of observed O₃ enhancements, and highlights the
681 value of utilising air mass back trajectories and modelling to interpret the source of O₃
682 enhancements where there are multiple emission sources.

683

684 **Acknowledgements**

685 The Cape Grim program, established by the Australian Government to monitor and study
686 global atmospheric composition, is a joint responsibility of the Bureau of Meteorology
687 (BOM) and the Commonwealth Scientific and Industrial Research Organisation (CSIRO).
688 We thank the staff at Cape Grim and staff at CSIRO Oceans and Atmosphere for providing
689 observation data for this work. Thank you to Nada Derek for producing figures, Mick Meyer
690 for providing fire scar information, and Suzie Molloy for providing advice on ozone
691 observation data. Finally we thank the three anonymous reviewers for their helpful
692 suggestions and comments

693

694 **References**

- 695 Akagi, S. K., Yokelson, R. J., Wiedinmyer, C., Alvarado, M. J., Reid, J. S., Karl, T.,
696 Crounse, J. D., and Wennberg, P. O.: Emission factors for open and domestic biomass
697 burning for use in atmospheric models, *Atmospheric Chemistry and Physics*, **11**, 4039-
698 4072, 10.5194/acp-11-4039-2011, 2011.
- 699 Akagi, S. K., Yokelson, R. J., Burling, I. R., Meinardi, S., Simpson, I., Blake, D. R.,
700 McMeeking, G. R., Sullivan, A., Lee, T., Kreidenweis, S., Urbanski, S., Reardon, J.,
701 Griffith, D. W. T., Johnson, T. J., and Weise, D. R.: Measurements of reactive trace gases
702 and variable O₃ formation rates in some South Carolina biomass burning plumes, *Atmos.*
703 *Chem. Phys.*, **13**, 1141-1165, 10.5194/acp-13-1141-2013, 2013.
- 704 Alvarado, M. J., and Prinn, R. G.: Formation of ozone and growth of aerosols in young
705 smoke plumes from biomass burning: 1. Lagrangian parcel studies, *Journal of*
706 *Geophysical Research*, **114**, 10.1029/2008jd011144, 2009.
- 707 Alvarado, M. J., Wang, C., and Prinn, R. G.: Formation of ozone and growth of aerosols
708 in young smoke plumes from biomass burning: 2. Three-dimensional Eulerian studies,
709 *Journal of Geophysical Research*, **114**, 10.1029/2008jd011186, 2009.
- 710 Alvarado, M. J., Lonsdale, C. R., Yokelson, R. J., Akagi, S. K., Coe, H., Craven, J. S.,
711 Fischer, E. V., McMeeking, G. R., Seinfeld, J. H., Soni, T., Taylor, J. W., Weise, D. R.,
712 and Wold, C. E.: Investigating the links between ozone and organic aerosol chemistry in

713 a biomass burning plume from a prescribed fire in California chaparral, *Atmos. Chem.*
714 *Phys.*, 15, 6667-6688, 10.5194/acp-15-6667-2015, 2015.

715 Anderson, D. C., Nicely, J. M., Salawitch, R. J., Canty, T. P., Dickerson, R. R., Hanisco,
716 T. F., Wolfe, G. M., Apel, E. C., Atlas, E., Bannan, T., Bauguitte, S., Blake, N. J., Bresch,
717 J. F., Campos, T. L., Carpenter, L. J., Cohen, M. D., Evans, M., Fernandez, R. P., Kahn,
718 B. H., Kinnison, D. E., Hall, S. R., Harris, N. R., Hornbrook, R. S., Lamarque, J. F., Le
719 Breton, M., Lee, J. D., Percival, C., Pfister, L., Pierce, R. B., Riemer, D. D., Saiz-Lopez,
720 A., Stunder, B. J., Thompson, A. M., Ullmann, K., Vaughan, A., and Weinheimer, A. J.:
721 A pervasive role for biomass burning in tropical high ozone/low water structures, *Nature*
722 *communications*, 7, 10267, 10.1038/ncomms10267, 2016.

723 Andreae, M. O., and Merlet, P.: Emission of trace gases and aerosols from biomass
724 burning, *Global Biogeochemical Cycles*, 15, 955-966, 10.1029/2000gb001382, 2001.

725 Andreae, M. O., Artaxo, P., Brandao, C., Carswell, F. E., Ciccioli, P., da Costa, A. L.,
726 Culf, A. D., Esteves, J. L., Gash, J. H. C., Grace, J., Kabat, P., Lelieveld, J., Malhi, Y.,
727 Manzi, A. O., Meixner, F. X., Nobre, A. D., Nobre, C., Ruivo, M., Silva-Dias, M. A.,
728 Stefani, P., Valentini, R., von Jouanne, J., and Waterloo, M. J.: Biogeochemical cycling
729 of carbon, water, energy, trace gases, and aerosols in Amazonia: The LBA-EUSTACH
730 experiments, *Journal of Geophysical Research-Atmospheres*, 107, 8066
731 10.1029/2001jd000524, 2002.

732 Arnold, S. R., Emmons, L. K., Monks, S. A., Law, K. S., Ridley, D. A., Turquety, S.,
733 Tilmes, S., Thomas, J. L., Bouarar, I., Flemming, J., Huijnen, V., Mao, J., Duncan, B. N.,
734 Steenrod, S., Yoshida, Y., Langner, J., and Long, Y.: Biomass burning influence on high-
735 latitude tropospheric ozone and reactive nitrogen in summer 2008: a multi-model
736 analysis based on POLMIP simulations, *Atmospheric Chemistry and Physics*, 15, 6047-
737 6068, 10.5194/acp-15-6047-2015, 2015.

738 Artaxo, P., Rizzo, L. V., Brito, J. F., Barbosa, H. M. J., Arana, A., Sena, E. T., Cirino, G.
739 G., Bastos, W., Martin, S. T., and Andreae, M. O.: Atmospheric aerosols in Amazonia
740 and land use change: from natural biogenic to biomass burning conditions, *Faraday*
741 *Discuss.*, 165, 203-235, 10.1039/c3fd00052d, 2013.

742 Azzi, M., Cope, M., and Rae, M.: Sustainable Energy Deployment within the Greater
743 Metropolitan Region. NSW- Environmental Trust 2012.

744 Barrett, D. J.: Steady state turnover time of carbon in the Australian terrestrial
745 biosphere, *Global Biogeochemical Cycles*, 16, 55-51-55-21, 10.1029/2002gb001860, 2002.

746 Broome, R. A., Cope, M. E., Goldsworthy, B., Goldsworthy, L., Emmerson, K., Jegasothy,
747 E., and Morgan, G. G.: The mortality effect of ship-related fine particulate matter in the
748 Sydney greater metropolitan region of NSW, Australia, *Environment International*, 87,
749 85-93, <http://dx.doi.org/10.1016/j.envint.2015.11.012>, 2016.

750 Castellanos, P., Boersma, K. F., and van der Werf, G. R.: Satellite observations indicate
751 substantial spatiotemporal variability in biomass burning NO_x emission factors for South
752 America, *Atmospheric Chemistry and Physics*, 14, 3929-3943, 10.5194/acp-14-3929-2014,
753 2014.

754 Cope, M., Lee, S., Noonan, J., Lilley, B., Hess, G. D., and Azzi, M.: Chemical Transport
755 Model - Technical Description, 2009.

756 Cope, M., Keywood, M., Emmerson, K., Galbally, I. E., Boast, K., Chambers, S., Cheng,
757 M., Crumeyrolle, S., Dunne, E., Fedele, R., Gillett, R., Griffiths, A., Harnwell, J., Katzfey,

758 J., Hess, D., Lawson, S. J., Miljevic, B., Molloy, S., Powell, J., Reisen, F., Ristovski, Z.,
759 Selleck, P., Ward, J., Zhang, C., and Zeng, J.: Sydney Particle Study Stage II., 2014.
760 <http://141.243.32.146/resources/aqms/SydParticleStudy10-13.pdf>

761 Cope, M. E., Hess, G. D., Lee, S., Tory, K., Azzi, M., Carras, J., Lilley, W., Manins, P. C.,
762 Nelson, P., Ng, L., Puri, K., Wong, N., Walsh, S., and Young, M.: The Australian Air
763 Quality Forecasting System. Part I: Project Description and Early Outcomes, *Journal of*
764 *Applied Meteorology*, 43, 649-662, doi:10.1175/2093.1, 2004.

765 Delaney, W., and Marshall, A. G.: Victorian Air Emissions Inventory for 2006, 20th
766 International Clean Air and Environment Conference, Auckland,, 2011.

767 Dennekamp, M., Straney, L. D., Erbas, B., Abramson, M. J., Keywood, M., Smith, K.,
768 Sim, M. R., Glass, D. C., Del Monaco, A., Haikerwal, A., and Tonkin, A. M.: Forest Fire
769 Smoke Exposures and Out-of-Hospital Cardiac Arrests in Melbourne, Australia: A Case-
770 Crossover Study, *Environmental health perspectives*, 123, 959-964, 10.1289/ehp.1408436,
771 2015.

772 Donahue, N. M., Robinson, A. L., Stanier, C. O., and Pandis, S. N.: Coupled Partitioning,
773 Dilution, and Chemical Aging of Semivolatile Organics, *Environmental Science &*
774 *Technology*, 40, 2635-2643, 10.1021/es052297c, 2006.

775 Draxler, R.R and Hess, G.D. : Description of the HYSPLIT_4 modeling system. NOAA
776 Technical Memorandum ERL ARL-224, Air Resources Laboratory Silver Spring,
777 Maryland, USA, 1997.

778 Emmerson, K. M., Galbally, I. E., Guenther, A. B., Paton-Walsh, C., Guerette, E. A.,
779 Cope, M. E., Keywood, M. D., Lawson, S. J., Molloy, S. B., Dunne, E., Thatcher, M., Karl,
780 T., and Maleknia, S. D.: Current estimates of biogenic emissions from eucalypts uncertain
781 for southeast Australia, *Atmos. Chem. Phys.*, 16, 6997-7011, 10.5194/acp-16-6997-2016,
782 2016.

783 Emmons, L. K., Apel, E. C., Lamarque, J. F., Hess, P. G., Avery, M., Blake, D., Brune,
784 W., Campos, T., Crawford, J., DeCarlo, P. F., Hall, S., Heikes, B., Holloway, J., Jimenez,
785 J. L., Knapp, D. J., Kok, G., Mena-Carrasco, M., Olson, J., O'Sullivan, D., Sachse, G.,
786 Walega, J., Weibring, P., Weinheimer, A., and Wiedinmyer, C.: Impact of Mexico City
787 emissions on regional air quality from MOZART-4 simulations, *Atmospheric Chemistry*
788 *and Physics*, 10, 6195-6212, 10.5194/acp-10-6195-2010, 2010.

789 Finch, D. P., Palmer, P. L., and Parrington, M.: Origin, variability and age of biomass
790 burning plumes intercepted during BORTAS-B, *Atmos. Chem. Phys.*, 14, 13789-13800,
791 10.5194/acp-14-13789-2014, 2014.

792 Ferek, R. J., Reid, J. S., Hobbs, P. V., Blake, D. R., and Lioussé, C.: Emission factors of
793 hydrocarbons, halocarbons, trace gases and particles from biomass burning in Brazil,
794 *Journal of Geophysical Research: Atmospheres*, 103, 32107-32118, 10.1029/98JD00692,
795 1998.

796 Flannigan, M. D., Krawchuk, M. A., de Groot, W. J., Wotton, B. M., and Gowman, L.
797 M.: Implications of changing climate for global wildland fire, *International Journal of*
798 *Wildland Fire*, 18, 483-507, <http://dx.doi.org/10.1071/WF08187>, 2009.

799 Fountoukis, C., and Nenes, A.: ISORROPIA II: a computationally efficient
800 thermodynamic equilibrium model for $K^+-Ca^{2+}-Mg^{2+}-NH_4^+-Na^+-SO_4^{2-}-NO_3^- -Cl^- -H_2O$
801 aerosols, *Atmos Chem Phys*, 7, 4639-4659, 2007.

802 Freitas, S. R., Longo, K. M., Chatfield, R., Latham, D., Silva Dias, M. A. F., Andreae, M.
803 O., Prins, E., Santos, J. C., Gielow, R., and Carvalho Jr, J. A.: Including the sub-grid
804 scale plume rise of vegetation fires in low resolution atmospheric transport models,
805 *Atmos. Chem. Phys.*, 7, 3385-3398, 10.5194/acp-7-3385-2007, 2007.

806 Galbally, I. E., Cope, M., Lawson, S. J., Bentley, S. T., Cheng, M., Gillet, R. W., Selleck,
807 P., Petraitis, B., Dunne, E., and Lee, S.: Sources of Ozone Precursors and Atmospheric
808 Chemistry in a Typical Australian City, 2008.
809 <http://olr.npi.gov.au/atmosphere/airquality/publications/pubs/ozone-precursors.pdf>

810 Galbally, I. E., Meyer, C. P., Bentley, S. T., Lawson, S. J., and Baly, S. B.: Reactive gases
811 in near surface air at Cape Grim, 2005-2006 – I E Galbally, C P Meyer, S T Bentley,
812 *Baseline Atmospheric Program Australia 2005-2006*, 77-79, 2007.

813 Giglio, L., Randerson, J. T., and van der Werf, G. R.: Analysis of daily, monthly, and
814 annual burned area using the fourth-generation global fire emissions database (GFED4),
815 *Journal of Geophysical Research: Biogeosciences*, 118, 317-328, 10.1002/jgrg.20042, 2013.

816 Gong, S. L.: A parameterization of sea-salt aerosol source function for sub- and super-
817 micron particles, *Global Biogeochem Cy*, 17, Artn 1097 Doi 10.1029/2003gb002079, 2003.

818 Gras, J. L.: Particles Program Report, *Baseline Atmospheric Program Australia 2005-*
819 *2006*, 85-86, 2007.

820 Goodrick, S. L., Achtemeier, G. L., Larkin, N. K., Liu, Y., and Strand, T. M.: Modelling
821 smoke transport from wildland fires: a review, *International Journal of Wildland Fire*,
822 22, 83, 10.1071/wf11116, 2013.

823 Hecobian, A., Liu, Z., Hennigan, C. J., Huey, L. G., Jimenez, J. L., Cubison, M. J., Vay,
824 S., Diskin, G. S., Sachse, G. W., Wisthaler, A., Mikoviny, T., Weinheimer, A. J., Liao, J.,
825 Knapp, D. J., Wennberg, P. O., Kurten, A., Crounse, J. D., St Clair, J., Wang, Y., and
826 Weber, R. J.: Comparison of chemical characteristics of 495 biomass burning plumes
827 intercepted by the NASA DC-8 aircraft during the ARCTAS/CARB-2008 field campaign,
828 *Atmospheric Chemistry and Physics*, 11, 13325-13337, 10.5194/acp-11-13325-2011, 2012.

829 Hess, G. D.: A photochemical model for air quality assessment: Model description and
830 verification, *Atmospheric Environment* (1967), 23, 643-660,
831 [http://dx.doi.org/10.1016/0004-6981\(89\)90013-9](http://dx.doi.org/10.1016/0004-6981(89)90013-9), 1989.

832 Hurley, P.: Development and Verification of TAPM, in: *Air Pollution Modeling and Its*
833 *Application XIX*, edited by: Borrego, C., and Miranda, A. I., Springer Netherlands,
834 Dordrecht, 208-216, 2008a.

835 Hurley, P. J.: TAPM V4. Part 1. Technical description, *CSIRO Marine and Atmospheric*
836 *Research Internal Report*, 2008b.

837 Jaffe, D. A., and Wigder, N. L.: Ozone production from wildfires: A critical review,
838 *Atmospheric Environment*, 51, 1-10, 10.1016/j.atmosenv.2011.11.063, 2012.

839 Jost, C., Trentmann, J., Sprung, D., Andreae, M. O., McQuaid, J. B., and Barjat, H.:
840 Trace gas chemistry in a young biomass burning plume over Namibia: Observations and
841 model simulations, *Journal of Geophysical Research-Atmospheres*, 108, 13, 8482
842 10.1029/2002jd002431, 2003.

843 Kaiser, J. W., Heil, A., Andreae, M. O., Benedetti, A., Chubarova, N., Jones, L.,
844 Morcrette, J. J., Razinger, M., Schultz, M. G., Suttie, M., and van der Werf, G. R.:

845 Biomass burning emissions estimated with a global fire assimilation system based on
846 observed fire radiative power, *Biogeosciences*, 9, 527-554, 10.5194/bg-9-527-2012, 2012.

847 Keywood, M., Guyes, H., Selleck, P., and Gillett, R.: Quantification of secondary organic
848 aerosol in an Australian urban location, *Environmental Chemistry*, 8, 115-126,
849 10.1071/en10100, 2011a.

850 Keywood, M., Kanakidou, M., Stohl, A., Dentener, F., Grassi, G., Meyer, C. P., Torseth,
851 K., Edwards, D., Thompson, A., Lohmann, U., and Burrows, J. P.: Fire in the Air-
852 Biomass burning impacts in a changing climate, *Critical Reviews in Environmental
853 Science and Technology*, DOI:10.1080/10643389.2011.6042482011b.

854 Keywood, M., Cope, M., Meyer, C. P. M., Iinuma, Y., and Emmerson, K.: When smoke
855 comes to town: The impact of biomass burning smoke on air quality, *Atmospheric
856 Environment*, 121, 13-21, <http://dx.doi.org/10.1016/j.atmosenv.2015.03.050>, 2015.

857 Korontzi, S., Ward, D. E., Susott, R. A., Yokelson, R. J., Justice, C. O., Hobbs, P. V.,
858 Smithwick, E. A. H., and Hao, W. M.: Seasonal variation and ecosystem dependence of
859 emission factors for selected trace gases and PM_{2.5} for southern African savanna fires,
860 *Journal of Geophysical Research: Atmospheres*, 108, n/a-n/a, 10.1029/2003JD003730,
861 2003.

862 Krummel, P. B., Fraser, P., Steele, L. P., Porter, L. W., Derek, N., Rickard, C., Dunse, B.
863 L., Langenfelds, R. L., Miller, B. R., Baly, S. B., and McEwan, S.: The AGAGE in situ
864 program for non-CO₂ greenhouse gases at Cape Grim, 2005-2006: methane, nitrous
865 oxide, carbon monoxide, hydrogen, CFCs, HCFCs, HFCs, PFCs, halons, chlorocarbons,
866 hydrocarbons and sulphur hexafluoride, *Baseline Atmospheric Program Australia 2005-
867 2006*, 2007.

868 Lawson, S. J., Keywood, M. D., Galbally, I. E., Gras, J. L., Caine, J. M., Cope, M. E.,
869 Krummel, P. B., Fraser, P. J., Steele, L. P., Bentley, S. T., Meyer, C. P., Ristovski, Z., and
870 Goldstein, A. H.: Biomass burning emissions of trace gases and particles in marine air at
871 Cape Grim, Tasmania, *Atmos. Chem. Phys.*, 15, 13393-13411, 10.5194/acp-15-13393-
872 2015, 2015.

873 Lei, W., Li, G., and Molina, L. T.: Modeling the impacts of biomass burning on air quality
874 in and around Mexico City, *Atmospheric Chemistry and Physics*, 13, 2299-2319,
875 10.5194/acp-13-2299-2013, 2013.

876 Lu, H., and Shao, Y. P.: A new model for dust emission by saltation bombardment, *J
877 Geophys Res-Atmos*, 104, 16827-16841, Doi 10.1029/1999jd900169, 1999.

878 Luhar, A. K., Mitchell, R. M., Meyer, C. P., Qin, Y., Campbell, S., Gras, J. L., and Parry,
879 D.: Biomass burning emissions over northern Australia constrained by aerosol
880 measurements: II—Model validation, and impacts on air quality and radiative forcing,
881 *Atmospheric Environment*, 42, 1647-1664,
882 <http://dx.doi.org/10.1016/j.atmosenv.2007.12.040>, 2008.

883 Mason, S. A., Trentmann, J., Winterrath, T., Yokelson, R. J., Christian, T. J., Carlson,
884 L. J., Warner, T. R., Wolfe, L. C., and Andreae, M. O.: Intercomparison of Two Box
885 Models of the Chemical Evolution in Biomass-Burning Smoke Plumes, *Journal of
886 Atmospheric Chemistry*, 55, 273-297, 10.1007/s10874-006-9039-5, 2006.

887 McGregor, J. L.: Recent developments in variable-resolution global climate modelling,
888 *Climatic Change*, 129, 369-380, 10.1007/s10584-013-0866-5, 2015.

889 Meyer, C. P., Luhar, A. K., and Mitchell, R. M.: Biomass burning emissions over
890 northern Australia constrained by aerosol measurements: I—Modelling the distribution
891 of hourly emissions, *Atmospheric Environment*, 42, 1629-1646,
892 <http://dx.doi.org/10.1016/j.atmosenv.2007.10.089>, 2008.

893 Ortega, A. M., Day, D. A., Cubison, M. J., Brune, W. H., Bon, D., de Gouw, J. A., and
894 Jimenez, J. L.: Secondary organic aerosol formation and primary organic aerosol
895 oxidation from biomass-burning smoke in a flow reactor during FLAME-3, *Atmospheric
896 Chemistry and Physics*, 13, 11551-11571, 10.5194/acp-13-11551-2013, 2013.

897 Pacifico, F., Folberth, G. A., Sitch, S., Haywood, J. M., Rizzo, L. V., Malavelle, F. F., and
898 Artaxo, P.: Biomass burning related ozone damage on vegetation over the Amazon forest:
899 a model sensitivity study, *Atmos. Chem. Phys.*, 15, 2791-2804, 10.5194/acp-15-2791-2015,
900 2015.

901 Parrington, M., Palmer, P. I., Henze, D. K., Tarasick, D. W., Hyer, E. J., Owen, R. C.,
902 Helmig, D., Clerbaux, C., Bowman, K. W., Deeter, M. N., Barratt, E. M., Coheur, P. F.,
903 Hurtmans, D., Jiang, Z., George, M., and Worden, J. R.: The influence of boreal biomass
904 burning emissions on the distribution of tropospheric ozone over North America and the
905 North Atlantic during 2010, *Atmospheric Chemistry and Physics*, 12, 2077-2098,
906 10.5194/acp-12-2077-2012, 2012.

907 Paugam, R., Wooster, M., Freitas, S., and Val Martin, M.: A review of approaches to
908 estimate wildfire plume injection height within large-scale atmospheric chemical
909 transport models, *Atmos. Chem. Phys.*, 16, 907-925, 10.5194/acp-16-907-2016, 2016.

910 Reid, C. E., Brauer, M., Johnston, F. H., Jerrett, M., Balmes, J. R., and Elliott, C. T.:
911 Critical Review of Health Impacts of Wildfire Smoke Exposure, *Environmental health
912 perspectives*, 124, 1334-1343, 10.1289/ehp.1409277, 2016.

913 Reid, J. S., Hyer, E. J., Prins, E. M., Westphal, D. L., Zhang, J., Wang, J., Christopher,
914 S. A., Curtis, C. A., Schmidt, C. C., Eleuterio, D. P., Richardson, K. A., and Hoffman, J.
915 P.: Global Monitoring and Forecasting of Biomass-Burning Smoke: Description of and
916 Lessons From the Fire Locating and Modeling of Burning Emissions (FLAMBE)
917 Program, *IEEE Journal of Selected Topics in Applied Earth Observations and Remote
918 Sensing*, 2, 144-162, 10.1109/JSTARS.2009.2027443, 2009.

919 Reisen, F., Meyer, C. P., McCaw, L., Powell, J. C., Tolhurst, K., Keywood, M. D., and
920 Gras, J. L.: Impact of smoke from biomass burning on air quality in rural communities
921 in southern Australia, *Atmospheric Environment*, 45, 3944-3953,
922 10.1016/j.atmosenv.2011.04.060, 2011.

923 Reisen, F., Duran, S. M., Flannigan, M., Elliott, C., and Rideout, K.: Wildfire smoke and
924 public health risk, *International Journal of Wildland Fire*, 24, 1029, 10.1071/wf15034,
925 2015.

926 Sarwar, G., Luecken, D., Yarwood, G., Whitten, G. Z., and Carter, W. P. L.: Impact of
927 an updated carbon bond mechanism on predictions from the CMAQ modeling system:
928 Preliminary assessment, *J Appl Meteorol Clim*, 47, 3-14, Doi 10.1175/2007jamc1393.1,
929 2008.

930 Sarwar, G., Appel, K. W., Carlton, A. G., Mathur, R., Schere, K., Zhang, R., and Majeed,
931 M. A.: Impact of a new condensed toluene mechanism on air quality model predictions
932 in the US, *Geosci Model Dev*, 4, 183-193, DOI 10.5194/gmd-4-183-2011, 2011.

933 Seinfeld, J. H., and Pandis, S. N.: Atmospheric chemistry and physics : from air pollution
934 to climate change, Wiley, New York, xxvii, 1326 p. pp., 1998.

935 Smagorinsky, J.: General circulation experiments with the primitive equations Monthly
936 Weather Review, 91, 99-164, doi:10.1175/1520-
937 0493(1963)091<0099:GCEWTP>2.3.CO;2, 1963.

938 Trentmann, J., Yokelson, R. J., Hobbs, P. V., Winterrath, T., Christian, T. J., Andreae,
939 M. O., and Mason, S. A.: An analysis of the chemical processes in the smoke plume from
940 a savanna fire, Journal of Geophysical Research-Atmospheres, 110, 20, D12301
941 10.1029/2004jd005628, 2005.

942 Tsimpidi, A. P., Karydis, V. A., Zavala, M., Lei, W., Molina, L., Ulbrich, I. M., Jimenez,
943 J. L., and Pandis, S. N.: Evaluation of the volatility basis-set approach for the simulation
944 of organic aerosol formation in the Mexico City metropolitan area, Atmos Chem Phys,
945 10, 525-546, 2010.

946 Urbanski, S. P.: Combustion efficiency and emission factors for wildfire-season fires in
947 mixed conifer forests of the northern Rocky Mountains, US, Atmos. Chem. Phys., 13,
948 7241-7262, 10.5194/acp-13-7241-2013, 2013.

949 van Leeuwen, T. T., and van der Werf, G. R.: Spatial and temporal variability in the ratio
950 of trace gases emitted from biomass burning, Atmospheric Chemistry and Physics, 11,
951 3611-3629, 10.5194/acp-11-3611-2011, 2011.

952 van Leeuwen, T. T., Peters, W., Krol, M. C., and van der Werf, G. R.: Dynamic biomass
953 burning emission factors and their impact on atmospheric CO mixing ratios, Journal of
954 Geophysical Research-Atmospheres, 118, 6797-6815, 10.1002/jgrd.50478, 2013.

955 Walcek, C. J.: Minor flux adjustment near mixing ratio extremes for simplified yet highly
956 accurate monotonic calculation of tracer advection, Journal of Geophysical Research:
957 Atmospheres, 105, 9335-9348, 10.1029/1999JD901142, 2000.

958 Wigder, N. L., Jaffe, D. A., and Saketa, F. A.: Ozone and particulate matter
959 enhancements from regional wildfires observed at Mount Bachelor during 2004-2011,
960 Atmospheric Environment, 75, 24-31, 10.1016/j.atmosenv.2013.04.026, 2013.

961 Yokelson, R. J., Bertschi, I. T., Christian, T. J., Hobbs, P. V., Ward, D. E., and Hao, W.
962 M.: Trace gas measurements in nascent, aged, and cloud-processed smoke from African
963 savanna fires by airborne Fourier transform infrared spectroscopy (AFTIR), Journal of
964 Geophysical Research-Atmospheres, 108, 8478 10.1029/2002jd002322, 2003.

965 Yokelson, R. J., Karl, T., Artaxo, P., Blake, D. R., Christian, T. J., Griffith, D. W. T.,
966 Guenther, A., and Hao, W. M.: The Tropical Forest and Fire Emissions Experiment:
967 overview and airborne fire emission factor measurements, Atmospheric Chemistry and
968 Physics, 7, 5175-5196, 2007.

969 Yokelson, R. J., Crouse, J. D., DeCarlo, P. F., Karl, T., Urbanski, S., Atlas, E., Campos,
970 T., Shinozuka, Y., Kapustin, V., Clarke, A. D., Weinheimer, A., Knapp, D. J., Montzka,
971 D. D., Holloway, J., Weibring, P., Flocke, F., Zheng, W., Toohey, D., Wennberg, P. O.,
972 Wiedinmyer, C., Mauldin, L., Fried, A., Richter, D., Walega, J., Jimenez, J. L., Adachi,
973 K., Buseck, P. R., Hall, S. R., and Shetter, R.: Emissions from biomass burning in the
974 Yucatan, Atmospheric Chemistry and Physics, 9, 5785-5812, 2009.

975 Yokelson, R. J., Burling, I. R., Urbanski, S. P., Atlas, E. L., Adachi, K., Buseck, P. R.,
976 Wiedinmyer, C., Akagi, S. K., Toohey, D. W., and Wold, C. E.: Trace gas and particle

977 **emissions from open biomass burning in Mexico, Atmospheric Chemistry and Physics,**
978 **11, 6787-6808, 10.5194/acp-11-6787-2011, 2011.**
979

980
981
982
983
984
985
986
987
988
989
990

Table 1. EF used in model sensitivity studies, corresponding to low (MCE=0.89), medium (MCE=0.92) and high (MCE = 0.95) MCEs. A subset of the total species included in the CB05 lumped chemical mechanism are shown. Also shown are savannah EF from Andreae and Merlet (2001) (A&M) and EF calculated from BB2 in previous work (Lawson et al., 2015). NO = nitric oxide, CO =carbon monoxide, PAR=paraffin carbon bond, OLE= terminal olefin carbon bond, TOL=toluene and other monoalkyl aromatics, XYL=xylene and other polyalkyl aromatics, BNZ =benzene, FORM=formaldehyde, ALD2=acetaldehyde, EC=elemental carbon <10 µm, OC=primary organic carbon < 10 µm

	EF g kg ⁻¹				
	A&M (2001) MCE 0.94	Lawson et al., (2015) MCE 0.88	Used in this work		
			MCE 0.89	MCE 0.92	MCE 0.95
NO	3.9	n/a	0.8	2.7	4.7
CO	65	127	121	89	57
PAR	1.55	n/a	2.33	2.02	1.40
OLE	0.54	n/a	0.81	0.7	0.49
TOL	0.2	0.30	0.3	0.26	0.18
XYL	0.045	0.26	0.07	0.06	0.04
BNZ	0.23	0.69	0.35	0.3	0.21
FORM	0.42	1.64	0.63	0.55	0.38
ALD2	0.5	0.92	0.75	0.65	0.45
EC	0.48	0.16	0.19	0.34	0.53
OC	3.40	n/a	5.10	4.08	3.06
NMOC/NO _x	1.60	n/a	11.99	2.97	1.20

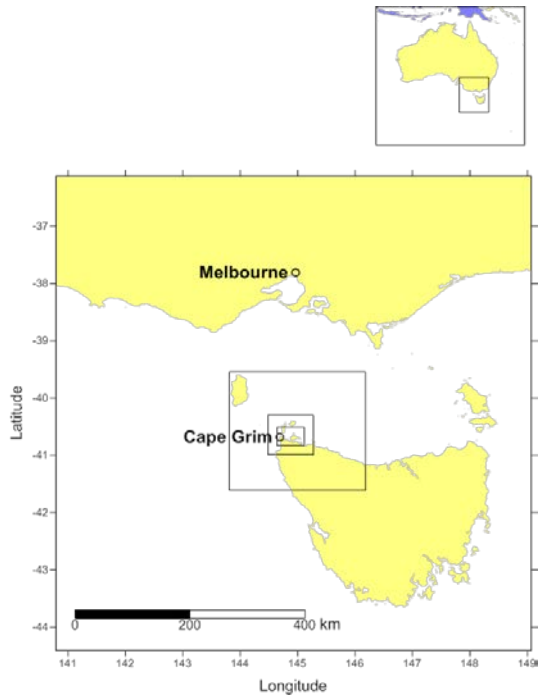
991

1 **Table 2. Summary of sensitivity study results, including Meteorology, Emission Factors and Spatial**
 2 **Variability.**

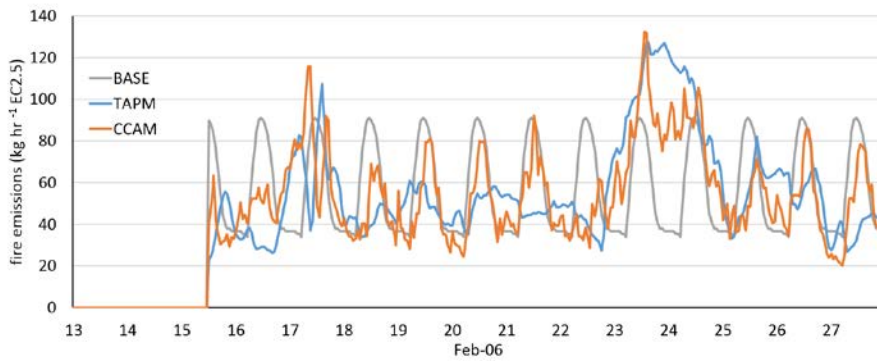
3
4

Sensitivity study	Species	TAPM-CTM simulation	CCAM-CTM simulation	Comments/drivers of model outputs
Meteorology (Section 3.1.1)	BC and CO	BB1 plume strike +3 hr Duration 12 hr (actual 5 hr)	BB1 plume strike -12 hr Duration 36 hr intermittent (actual 5 hr)	Narrow BB plume. Differences in plume strike due to timing of wind direction change; windspeeds; direct or indirect advection of plume over Cape Grim
		BB2 plume strike -26 hr Duration 50 hr (actual 29 hr)	BB2 plume strike -26 hr Duration 57 hr (actual 29 hr)	Wind direction differences driven by gravity wave oscillations; timing of wind direction change; different wind speeds driving absolute BB emissions and plume dispersion
	O ₃	4 O ₃ peaks simulated (2 observed, 2 not)	1 O ₃ peak simulated (observed)	Differences in simulated wind speed and direction (and EF – see below)
Emission Factors (Section 3.1.2)	BC and CO	BC peak magnitude varies by factor 3, CO factor 2 with different EF runs	As for TAPM-CTM	Concentrations vary according to EF input ratios.
	O ₃	2 peaks with high EF sensitivity, 2 peaks with no EF sensitivity	1 peak with no EF sensitivity	Different NMOC/NO _x emission ratios (varies with MCE) drives destruction or production of O ₃ in fire related peaks. MCE 0.89 TAPM-CTM simulation gives best agreement with observations
Spatial Variability (Section 3.1.3)	CO	Differences of up to > 500 ppb in grid points 1 km apart (BB2)	n/a	Narrow BB plume
	O ₃	Differences of up to 15 ppb in grid points 1 km apart (BB1)	n/a	Narrow ozone plume generated downwind of fire

5

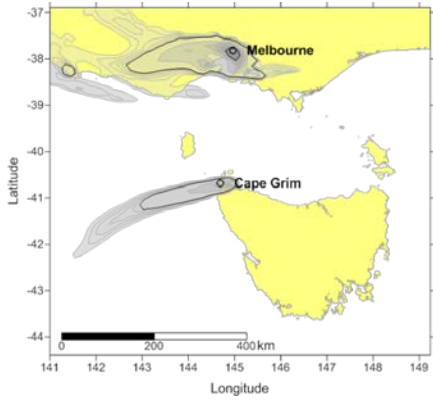


6
 7 **Figure 1. The five nested computational domains used in TAPM-CTM and CCAM-CTM, showing cell**
 8 **spacings of 20 km, 12 km, 3 km, 1 km and 400 m.**



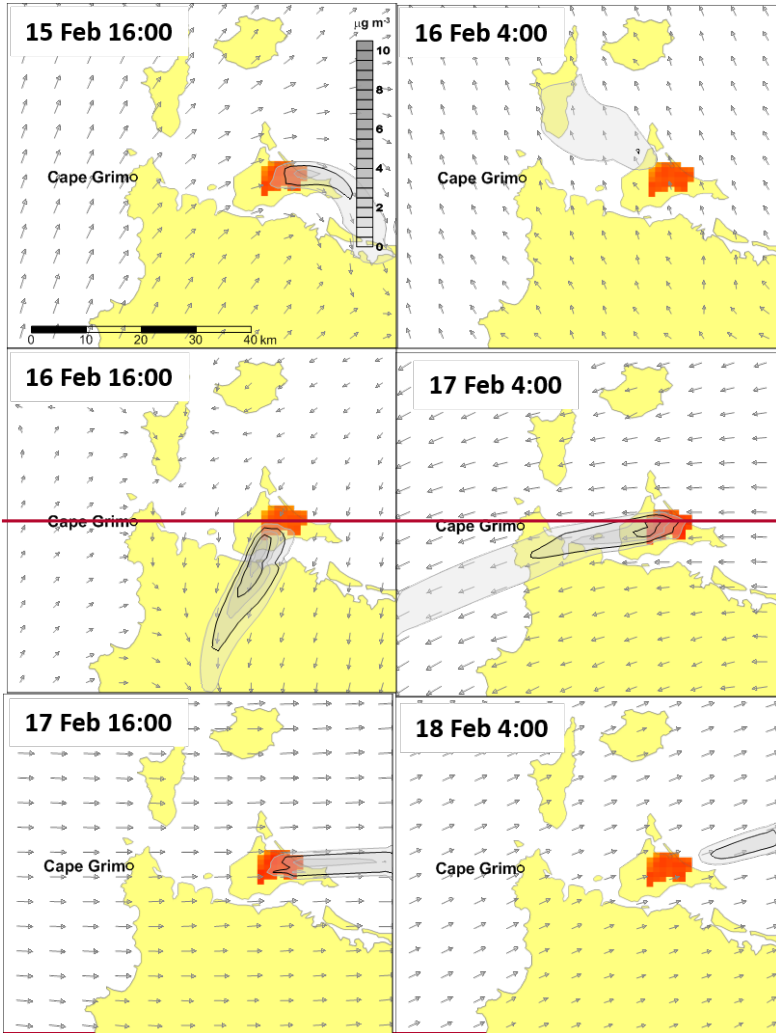
9
 10 **Figure 2 Base hourly diurnal emissions and revised Macarthur Fire Danger Index (FDI)-scale emissions**
 11 **generated using TAPM and CCAM meteorology.**
 12

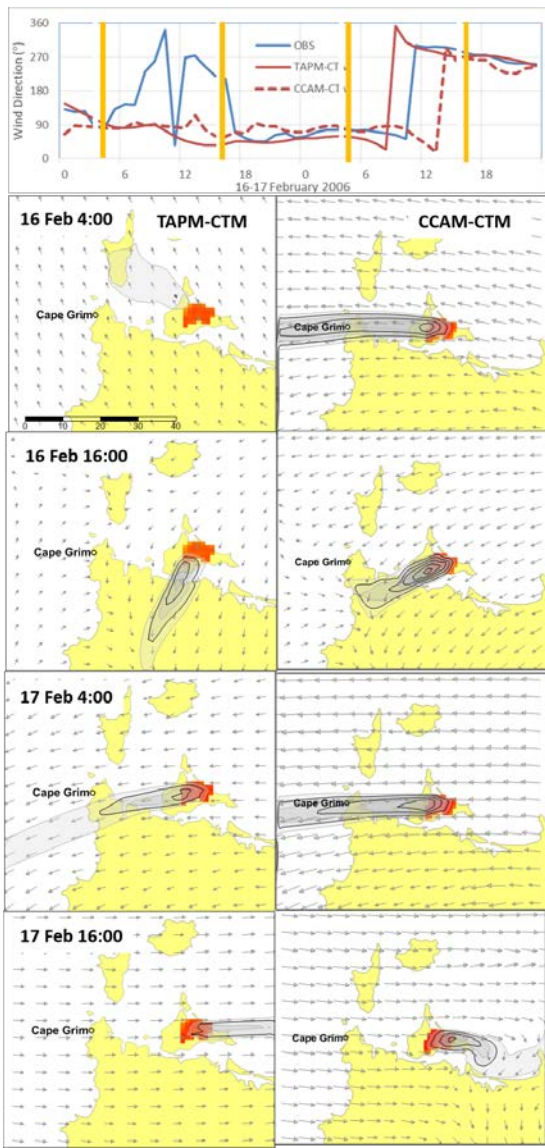
13



14

15 **Figure 3. Model output of BC (left) on the 23rd February, with a MODIS Truecolour image of the same**
16 **period.**





18

19 **Figure 4. Model concentration isopleth of BC for TAPM-CTM (left panels) and CCAM-CTM (right panels).**
 20 **Panels show Model output of BC for TAPM-CTM at 12 hour time intervals during BB1, showing including**
 21 **the Robbins Island BB plume intermittently striking Cape Grim, and then the change in plume direction**
 22 **with wind direction change. Arrows are wind vectors. The time series of observed and modelled wind**
 23 **direction for BB1 is shown above with orange bands highlighting the periods corresponding to the panels.**

Formatted: Not Highlight

Formatted: Not Highlight

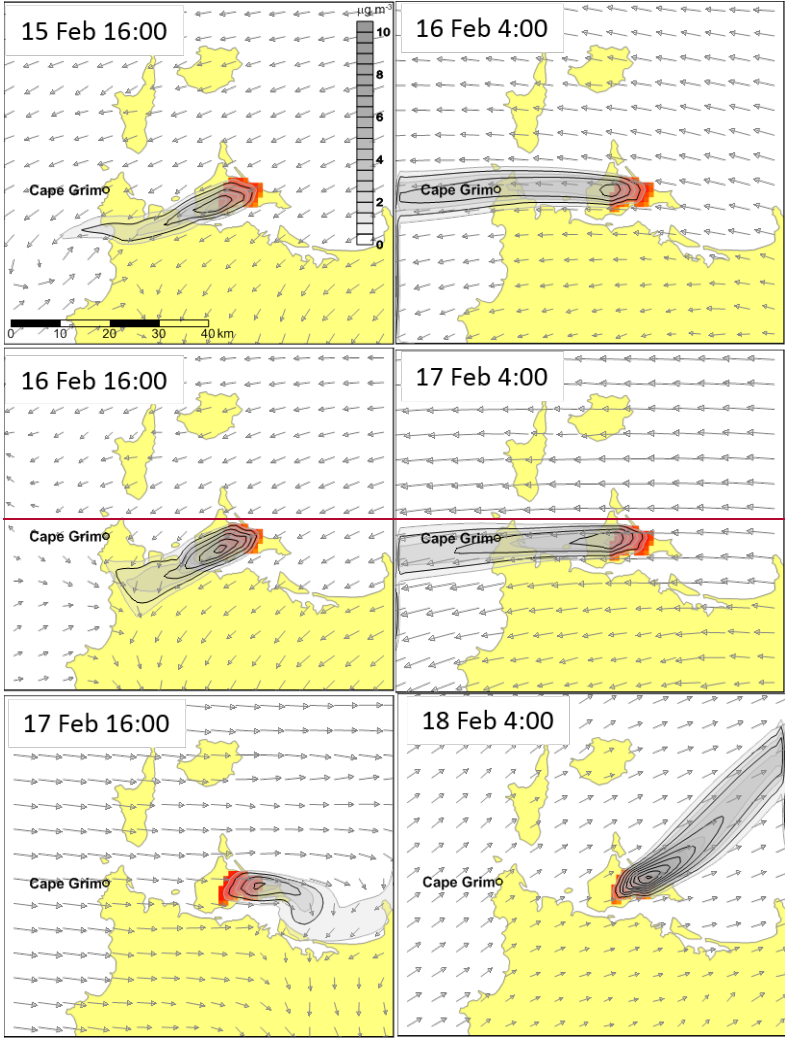
Formatted: Not Highlight

24 ~~Model output of BC for CCAM-CTM at 12-hour time intervals during BB1, showing the Robbins Island~~
25 ~~BB plume intermittently striking Cape Grim, and then the change in plume direction with wind direction~~
26 ~~change. Arrows are wind vectors.~~

27

28

Formatted: Normal



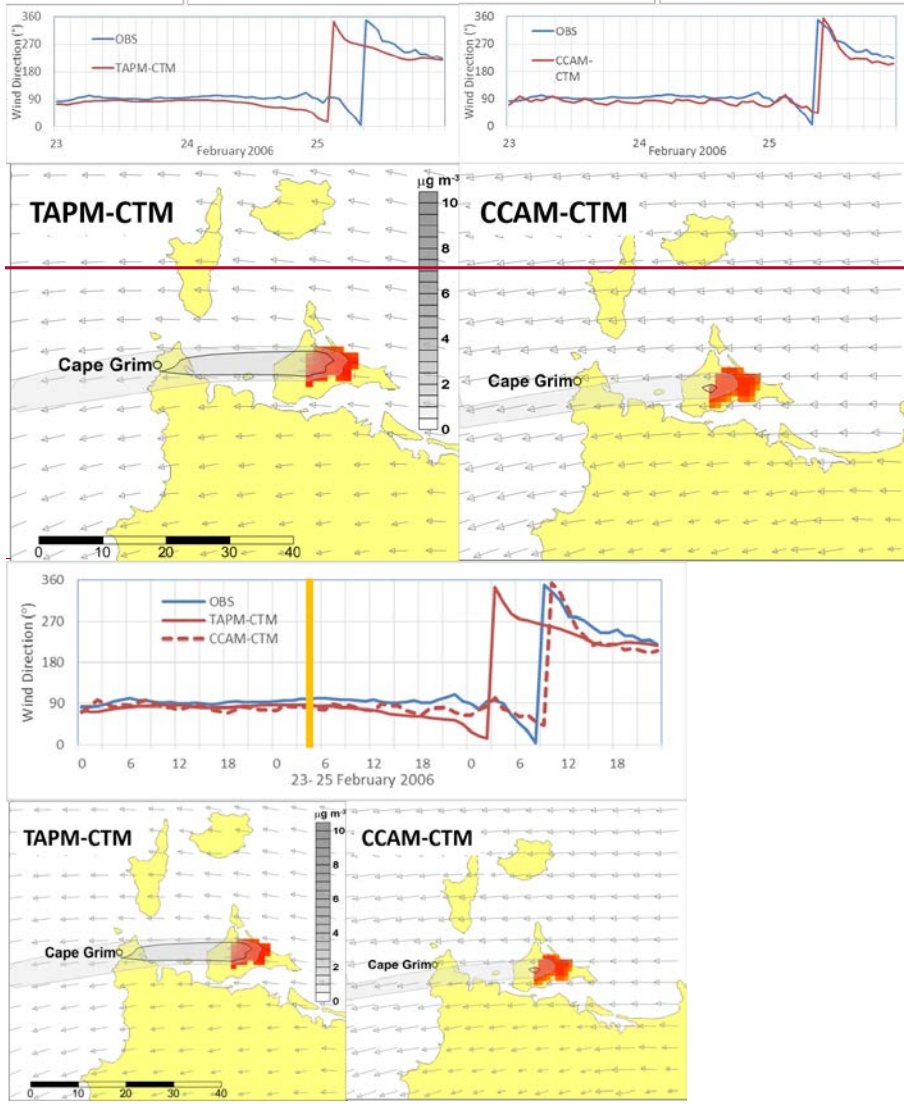
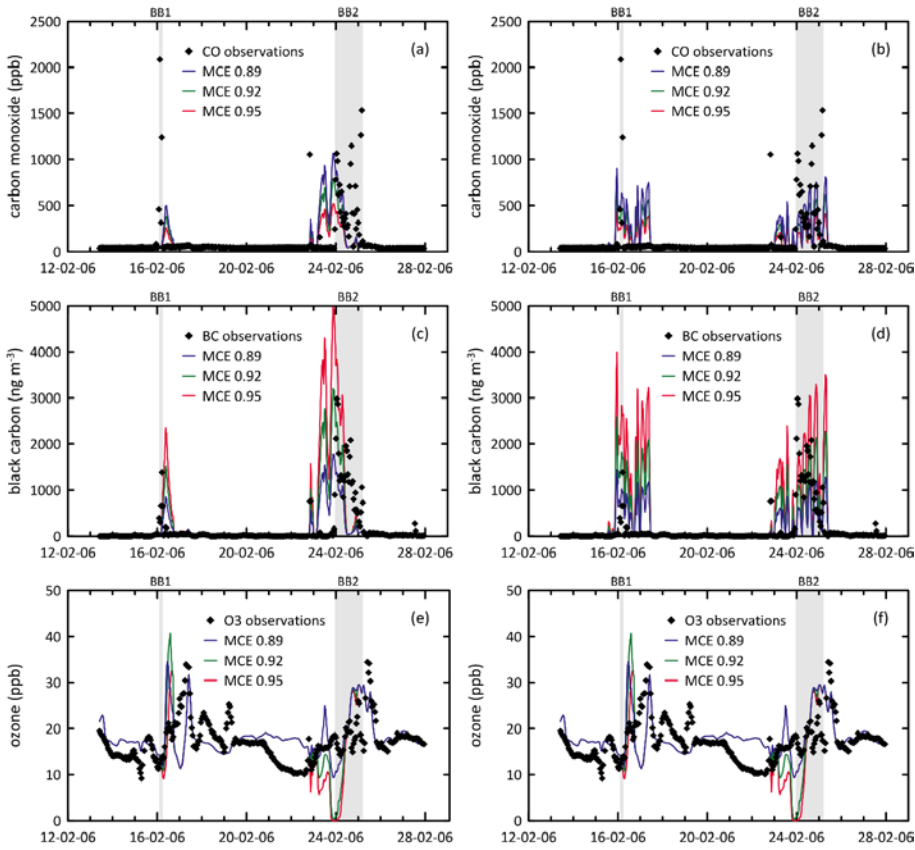


Figure 5 Model concentration isopleth of BC and Wind direction for TAPM-CTM and CCAM-CTM at 05:00 on the 24 February during BB2. Arrows are wind vectors. The time series of observed and modelled wind direction for BB2 is shown above with an orange band highlighting the period corresponding to the panels.

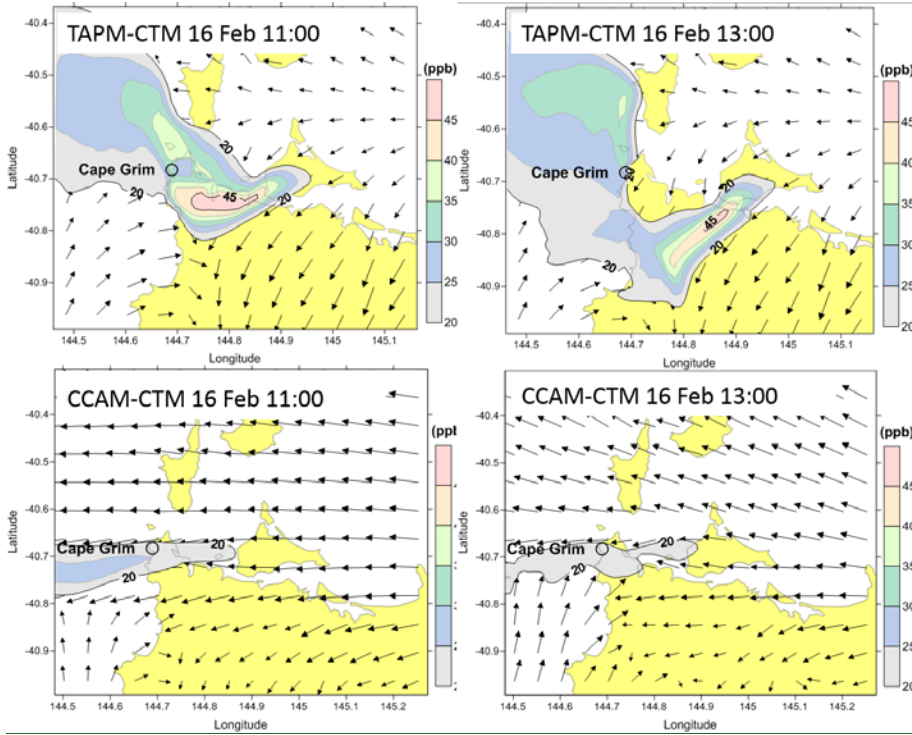
Formatted: Not Highlight

Formatted: Not Highlight



38
 39 **Figure 6. Simulated CO using a) TAPM-CTM and b) CCAM-CTM, simulated BC using c) TAPM-CTM**
 40 **and d) CCAM-CTM, and simulated O₃ using e) TAPM-CTM and f) CCAM-CTM. Coloured lines represent**
 41 **different MCE EF simulations, black symbols are observations**

42



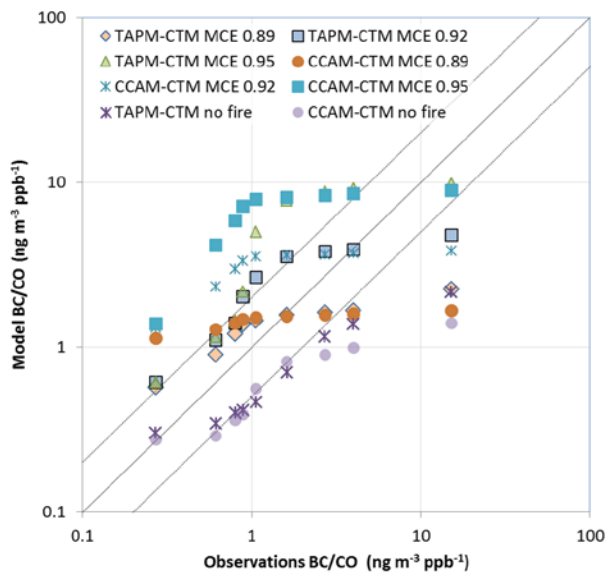
43

44 **Figure 7** Model output showing O₃ enhancement downwind of the fire during BB1 at 11:00 and 13:00 on
45 the 16 February for TAPM-CTM (top) and CCAM-CTM (bottom). The spatially variable plume and
46 complex wind fields are shown. Arrows are wind vectors.

47

Formatted: Keep with next

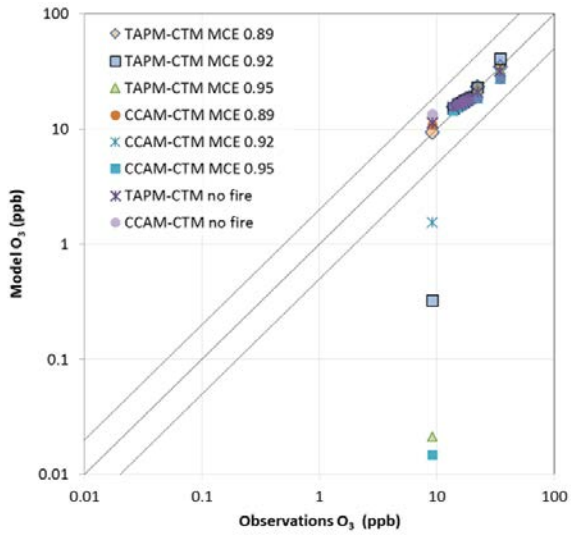
Formatted: Caption



48

49 **Figure 8** Quantile-quantile plots of observed and modelled BC/CO ratios for the TAPM-CTM and CCAM-
 50 CTM simulations. For each scenario, the model-data pairs correspond to the following percentiles- 0.2, 0.3,
 51 0.4, 0.5, 0.6, 0.7, 0.8, 0.9 and 1. Note log scale on both axes. Solid line is 1:1 and dotted lines show performance
 52 within a factor of two.

Formatted: Keep with next



53

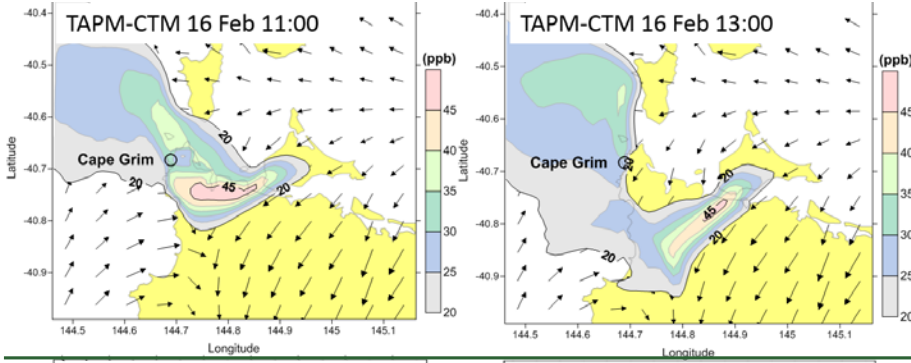
54 **Figure 9** Quantile-quantile plots of observed and modelled O₃ for the TAPM-CTM and CCAM-CTM
 55 simulations. For each scenario, the model-data pairs correspond to the following percentiles- 0.2, 0.3, 0.4,
 56 0.5, 0.6, 0.7, 0.8, 0.9 and 1. Note log scale on both axes. Solid line is 1:1 and dotted lines show performance
 57 within a factor of two.

58

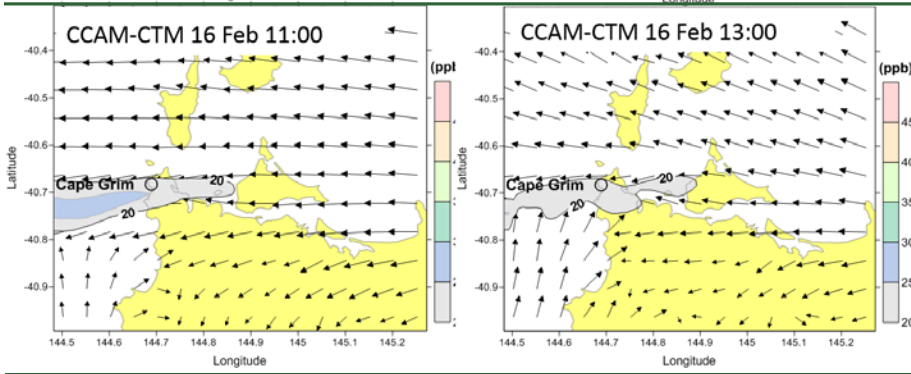
Formatted: Keep with next

Formatted: Caption

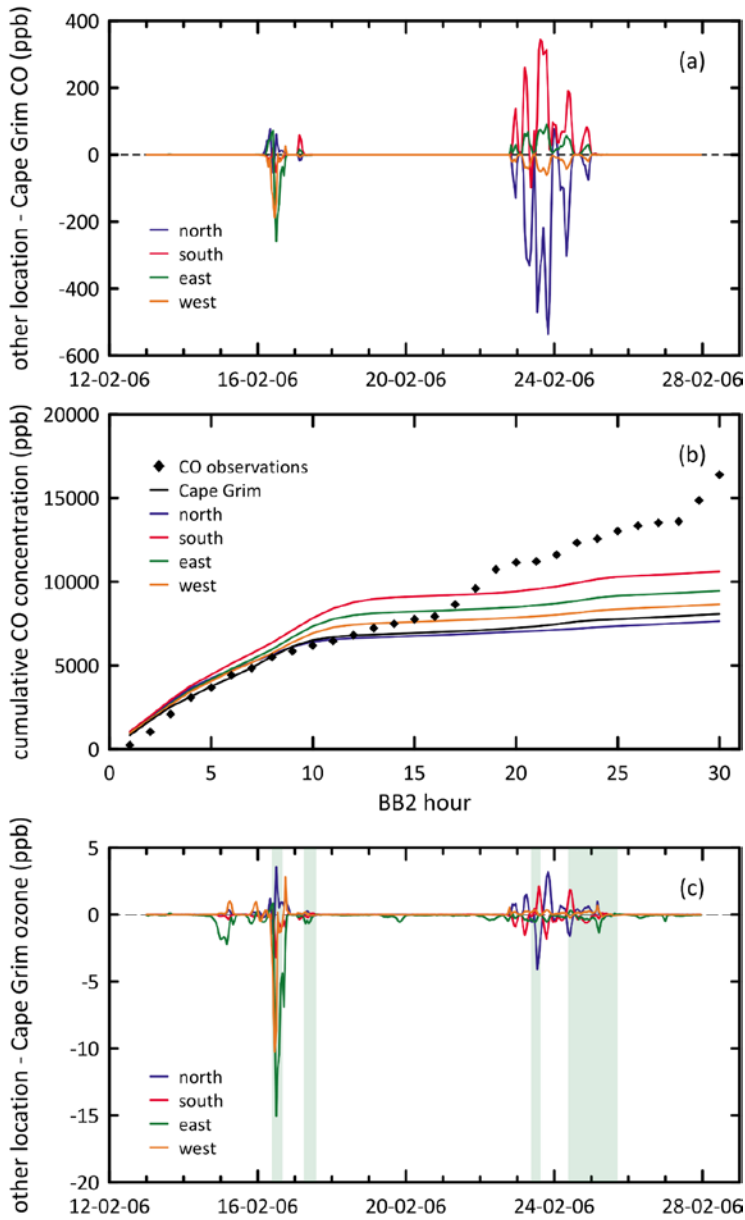
59



60



61

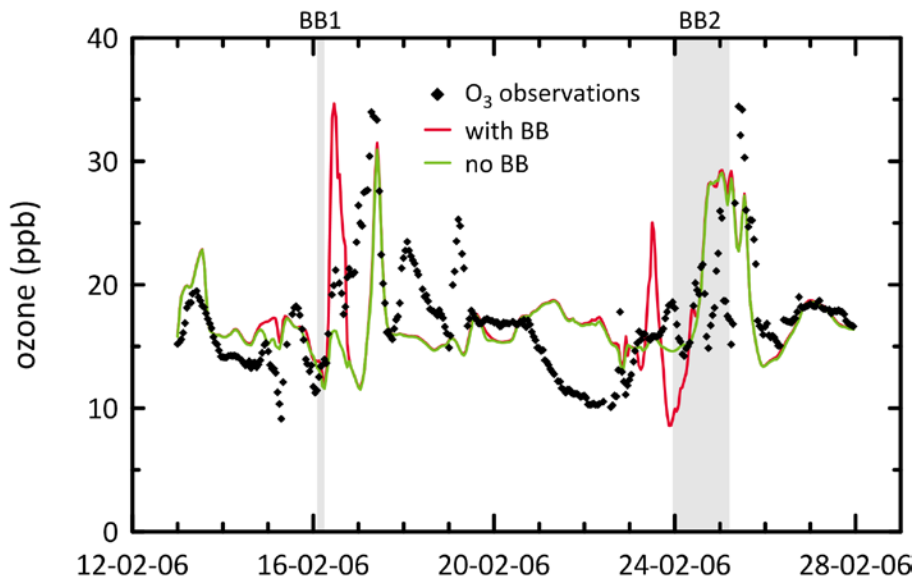


62
 63 **Figure 10** Simulated spatial variability using TAPM-CTM with MCE=0.89 showing a) time series of CO
 64 over two weeks of fire (BB1 and BB2 shown), b) the observed and modelled cumulative concentration of
 65 CO over the 29 hour duration of BB2 and c) time series of O₃ over the two weeks of fire. The four modelled
 66 O₃ peaks in the Cape Grim gridpoint are shaded. Figs a and c show the difference between simulated

67 concentrations at Cape Grim and at 4 surrounding grid points 1km north, south, east and west of Cape
68 Grim. Fig b shows simulated cumulative CO at Cape Grim and at 4 surrounding grid points. . Observations
69 are black symbols.

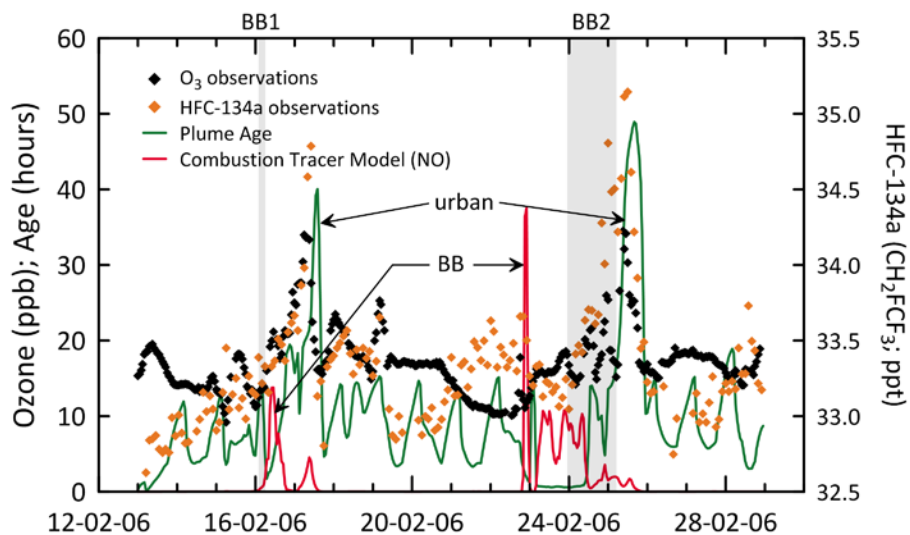
70

71



72

73 Figure 11 Simulated O₃ concentration at Cape Grim with the Robbins Island fire emissions (red line) and
74 without the fire emissions (green line). Observations are black symbols. Model used was TAPM-CTM with
75 EF corresponding to MCE=0.89. The periods corresponding to observed BB1 and BB2 are shaded.



76
 77 **Figure 12** Simulated plume age (green line), simulated combustion tracer (NO) (red line), observed O₃
 78 (black symbols) and observed HFC-134a (orange symbols) over 2 week duration of the fire. The modelled
 79 **BB** periods (red peaks) and impact of urban air from mainland Australia (green peaks) are labelled. The
 80 periods corresponding to observed BB1 and BB2 are shaded.

81
 82
 83
 84
 85 End
 86
 87
 88
 89